

Disorder effect on 3-dimensional  $Z_2$  quantum spin Hall systemsRyuichi Shindou<sup>1</sup> and Shuichi Murakami<sup>2,3</sup><sup>1</sup>Furusaki Condensed Matter Theory Laboratory, RIKEN, 2-1 Hirosawa, Wako, Saitama 351-0198, Japan<sup>2</sup>Department of Physics, Tokyo Institute of Technology,  
2-12-1 Ookayama, Meguro-ku, Tokyo 152-8551, Japan<sup>3</sup>PRESTO, Japan Science and Technology Agency (JST), Kawaguchi, Saitama 332-0012, Japan

In this paper, we address ourselves to the nonmagnetic disorder effects onto the quantum critical point which intervenes the 3-dimensional  $Z_2$  quantum spin Hall insulator (topological insulator) and an ordinary insulator. The minimal model describing this type of the quantum critical point is the single-copy of the 3+1 Dirac fermion, whose topological mass induces the phase transition between the topological insulator and an ordinary one. We first derive the phase diagram spanned by the mass term  $m$ , chemical potential and strength of the disorder within the self-consistent Born approximation. By way of this, we find a finite density of state appears even at the zero-energy and at the phase transition point, i.e.  $m = 0$ , if the strength of the disorder potential exceeds some critical value. To infer the structure of the low-energy effective theory around these zero-energy states, we further calculated the weak localization (WL) correction to the conductivity. To be more specific, we have found that the diffusion is dominated by the charge diffusion mode and parity diffusion mode. While the charge diffusion mode always carries the diffusion pole, the parity diffusion mode becomes massless only at  $m = 0$ , but suffers from the infrared cutoff for non-zero  $m$ . Corresponding to this feature of the diffusion, the Cooperon is also composed of two quasi-degenerate contributions. We found that these two give rise to the same magnitude of the anti-weak-localization (AWL) correction with each other at  $m = 0$ . As a result, when the topological mass is re-tuned to be zero (but for generic), the AWL correction becomes doubled (quantum correction doubling). Based on this observation, we will discuss the possible microscopic picture of the "levitation and pair annihilation" phenomena, recently discovered by Onda et al.<sup>26</sup>.

PACS numbers:

## I. INTRODUCTION

Physics of spin transport has been a matter of intensive research in recent years. One of the topics of current interest is the spin Hall effect. This has been originally proposed theoretically<sup>1,2</sup> and later followed by various experimental results<sup>3,4</sup>. The research on the spin Hall effect opens a new field of Hall effects in time-reversal-invariant systems. This has also led us to a new concept of the quantum spin Hall effect, which is the natural "spin" extension of the quantum Hall effect<sup>5,6,7</sup>. In the quantum spin Hall effect in two dimensions, the bulk is gapped while there are gapless edge states carrying spin current. In this case, the external magnetic field is zero, while the spin-orbit coupling acts as a "spin-dependent magnetic field", giving rise to the effect analogous to the quantum Hall effect. Such insulators showing the quantum spin Hall effect are characterized by the  $Z_2$  topological number<sup>5</sup>. We shall call them as  $Z_2$  quantum spin Hall insulators (QSHI).

The simplest system for the two-dimensional (2-d)  $Z_2$  QSHI is realized as a superposition of the wavefunctions of two quantum Hall subsystems<sup>5,6,7</sup>, one with spin up and the other with spin down, having opposite Chern numbers. The system respects not only the time-reversal (T) invariance but also the spin-conservation. Such an insulator supports the same numbers of right-moving up-spin edge states and left-moving down-spin edges.

This Kramers pair of chiral edge states is often called as the helical edge state. By its construction, the num-

ber of this Kramers pairs of edge states correspond to the Chern integer associated with its bulk wavefunction<sup>8</sup>. The T symmetry guarantees the double degeneracy between right-moving up-spin and left-moving down-spin states. Thus, the stability of each Kramers pair is supported by this T symmetry.

Spin non-conserving (but T invariant) perturbations, however, introduce level repulsions between two different Kramers pairs. Namely, they usually let two pairs annihilate with each other, and open a gap. Accordingly, in the presence of generic spin-non-conserving perturbations, those wavefunctions having even numbers of Kramers pairs, reduce to trivial insulators, which have no gapless edge states<sup>9,10,11,12</sup>. Meanwhile, wavefunctions having odd numbers of pairs still can have one active helical edge mode. The latter is dubbed as the  $Z_2$  quantum spin Hall (topological) insulator. Thus, stability of such a gapless edge state is protected only by the T symmetry, while does not require spin-conservations anymore<sup>9,10,11,12,13,14</sup>.

The three-dimensional (3-d) version<sup>15,16,17,18,19,21</sup> of the  $Z_2$  QSHI carries same characters as that of 2-d does. The 3-d  $Z_2$  QSHI also allows any spin-nonconserving perturbations, while always requires the T symmetry. Simultaneously, however, it is not a mere extension of the 2-d  $Z_2$  QSHI, in a sense that 3-d  $Z_2$  QSHI has no U(1)-analogue of QSHI. Namely, they support a 2+1 massless Dirac fermion as its surface state<sup>15,19</sup>, instead of a helical edge state. In the 2-d surface Brillouin zone, say  $k_x$ - $k_y$  plane, this massless Dirac fermion has a spin which de-

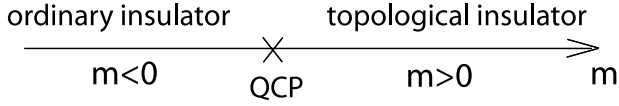


FIG. 1: A schematic phase diagram for the quantum critical point intervening the  $Z_2$  QSHI and an ordinary insulator.  $m$  is a system parameter driving the phase transition. When  $m = 0$ , the system is in a critical phase. In the Fu-Kane-Mele model, it corresponds to the relative strength of one out of the four NN transfer integrals emitting from a single site.

depends on the (surface) crystal momentum. It is clear that such an insulator cannot be adiabatically connected into a composite of two spinless wavefunctions. In such  $Z_2$  QSHI, the  $T$  symmetry therefore guarantees the massless nature of each  $2+1$  surface Dirac fermion.

$Z_2$  QSHI always has a quantum critical point at its phase boundary to any ordinary insulators, in both 2-d and 3-d. For example, from the 3-d tight-binding model proposed by Fu, Kane and Mele<sup>15</sup>, we can explicitly see this; when a certain  $T$  symmetric parameter is varied in their model, 3d  $Z_2$  QSHI is driven into an ordinary insulator, latter of which does not support any surface states (see Fig. 1). Observing this, a following question naturally arises; during this tuning, the  $T$  symmetry is always preserved, so that the massless nature of the surface Dirac fermion is supposed to be protected by this. At the same time, however, this  $2+1$  surface fermion should have become "massive", when a system enters an ordinary insulator phase. Thus, one might ask how this single surface Dirac fermion could acquire a finite mass, with keeping the  $T$  symmetry?

The answer is simple; we have two sample boundaries, say  $z = +L$  and  $z = -L$ . Each boundary supports one  $2+1$  surface massless Dirac fermion respectively. They are localized at each boundary, when the bulk gap is sufficiently large. In such a situation, a mixing between these two  $2+1$  surface massless Dirac fermions is tiny, i.e.  $O(e^{-L/\xi})$  with  $\xi$  being the localization length. However, when a system becomes close to the quantum critical point, a mixing between these two surface states becomes substantial, with increasing  $L$ . When a bulk eventually reaches the quantum critical point, two surface massless Dirac fermions readily communicate via extended bulk states. Thus, they generally annihilate in pairs, just as in those insulators having even number of  $2+1$  surface Dirac fermions at one boundary.

This simple picture in the clean limit raises the following non-trivial speculations about the disorder effects on the  $Z_2$  QSHI. Suppose that  $T$ -symmetric random potentials are introduced in the topological insulator phase. When the corresponding bulk gap is sufficiently large, we could begin with two separate bands. The scaling argument in 3-d<sup>22</sup> tells us that each band should always have two mobility edges, respectively (see Fig. 2(b)). Namely, there is no delocalized bulk-wavefunction near

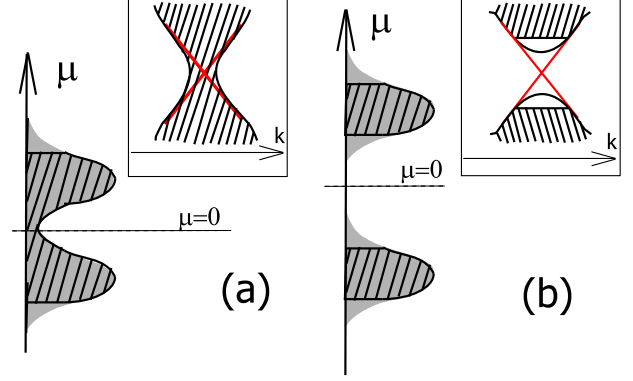


FIG. 2: A schematic picture of the density of state and mobility edges, where hatched region corresponds to the extended state. Inset represents the energy dispersion as a function of surface crystal momentum, where the red line corresponds to the surface state at  $z = L$ . (a)  $m = 0$ ; at quantum critical point. (b)  $m > 0$ ; in the topological insulator phase.

the zero energy. Starting from this phase, let us change some  $T$ -invariant model-parameters, so that a bulk transits from this topological insulator to an ordinary one. From the argument in the clean limit, one can then expect that a delocalized bulk-wavefunction should emerge at the zero-energy region at the quantum critical point, i.e.  $m = 0$  (see Fig. 2(a)). If it were not, the two surface states localized at the two sample boundaries could not communicate at all and they could not annihilate with each other. As a result, the system was unable to smoothly enter an ordinary band insulator, since the latter one does not support any surface state at all.

To put this reversely, the existence of the quantum critical point (QCP) having extended bulk wavefunctions is always required, whenever this critical point separates an ordinary insulator and the topological insulator. This is because these two insulating phases support different numbers of Kramers pairs of surface states. Moreover, provided that these surface states are stable by itself, this QCP should be also stable, however small the density of state (DOS) at the zero energy is and however strong the disorder strength is. Otherwise, the topological insulator could be adiabatically connected into an ordinary band insulator, which contradicts the different  $Z_2$  topological numbers for the two phases.

In this paper, we will uncover several novel features associated with the non-magnetic disorder effects onto this topological quantum critical point. The organization of this paper is summarized as follows. In the next section, we will briefly review the effective continuum model for the quantum critical point intervening the  $Z_2$  topological insulator and an ordinary insulator. The effective model is known to be described by the  $3+1$  Dirac fermion, whose mass term brings about the topological quantum phase transition. Namely, when the mass term changed from positive to negative, a system transits from the topolog-

ical insulator to an ordinary insulator. As such, we call this mass term especially as the topological mass term. Based on this effective model, we will next introduce various types of the on-site random potentials respecting the  $T$ -symmetry. Note that, in this paper, we restrict ourselves to  $T$ -symmetric cases and exclude magnetic impurities, because, in the absence of the  $T$ -symmetry, the two phases are no longer topologically distinct.

Based on the self-consistent Born approximation, we first work over the single-particle Green function in the section III. The phase diagram spanned by the (bare) chemical potential  $\mu$ , (bare) mass term  $m$  and strength of the disorder  $\Gamma$  is derived. In particular, at the critical point, i.e.  $m = 0$ , we found some critical value of the disorder strength,  $\Gamma_c$ , above which the zero-energy state, i.e.  $\epsilon = 0$ , acquires a finite lifetime;

$$\frac{1}{\Gamma_c} \text{Arctan} \frac{\Gamma_c}{2} = 1 - \frac{c}{2}; \quad (1)$$

Since the density of state in our model is always proportional to the inverse of the lifetime (see below), non zero  $\Gamma^{-1}$  simply means that a system is in a compressible phase.

When a finite but small topological mass  $m$  is introduced for  $\Gamma > \Gamma_c$ , the lifetime  $\tau$  and the renormalized mass  $\bar{m}$  becomes as follows;

$$\frac{1}{\bar{m}} = \frac{1}{\frac{\Gamma}{2}} - \frac{m^2}{4} + \frac{m}{2}; \quad (2)$$

where  $\Gamma_0$  is given as a function only of  $\Gamma$  via Eq. (1). Thus, when the bare topological mass exceeds the critical value  $m_c = \Gamma_0^{-1}$ , the density of state vanishes, so that a system enters an incompressible phase. This gapped phase can be adiabatically connected into band insulator phases in the clean limit. Accordingly, we will reach the phase diagram for the zero-energy state as depicted in Fig. 3. In the section III, we also describe the behavior of the one-particle Green function for a finite  $\Gamma$  (see below), in which we observe that the compressible phase (not necessarily metallic phase) always intervenes the topological insulator phase and an ordinary insulator phase as in Fig. 3.

Focusing on this intervening compressible phase, especially for  $\Gamma < \Gamma_c$ , we will derive in the section. IV the diffusion, Cooperon and the weak localization correction to the electric conductivity. We will first observe that the diffusion is composed of two quasi-degenerate low-energy modes;

$$\hat{G}^d(q;!) / [! + iDq^2]^{-1} + \frac{1}{! + iDq^2 + i\frac{1}{\tau_{\text{topo}}}} \hat{G}_2^d +$$

(see Fig. (11) or eq. (74) for the definition of  $\hat{G}^d(q;!)$ ). The first term participates in usual charge diffusion mode, and therefore always has the diffusion pole, i.e.  $[! + iDq^2]^{-1}$  (! and  $q$  stand for the frequency and momentum

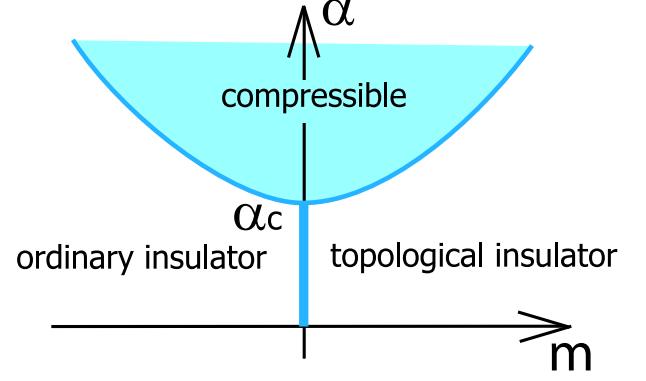


FIG. 3: A schematic phase diagram for  $\Gamma = 0$ . A blue shaded region corresponds to a compressible phase, which separates two gapped phases, i.e. an ordinary insulator and the topological insulator. This phase boundary for  $\Gamma > \Gamma_c$  is given by  $1 - \frac{c}{2} = \frac{\Gamma}{2} \text{Arctan} \frac{\Gamma}{m}$ .

of the density fluctuation respectively). The other low-energy mode, however, becomes massless only in the absence of the topological mass. Namely, its low-energy and long wavelength behavior is generally truncated by the infrared cutoff  $\frac{1}{\tau_{\text{topo}}}$ , while this infrared cutoff reduces to zero at  $m = 0$  (but generic), i.e.  $\frac{1}{\tau_{\text{topo}}} \propto m^2$ .

Physically speaking, this second mode describes the diffusion of the parity density degree of freedom, which becomes a conserved quantity of our effective Hamiltonian at  $m = 0$ . Namely, the parity-density correlation function exhibits the diffusion pole structure at the critical point ( $m = 0$ ), while it becomes massive in the presence of the finite topological mass. Consequently, the diffusion acquires one additional low-energy, i.e. the 2nd term of eq. (3), into which the information of this parity-density correlation function is separately encoded.

When the hole-line of the diffusion time-reversed, these two-mode features are transcribed into the Cooperon: the Cooperon thus obtained is also composed of two quasi-degenerate dominant contributions;

$$\hat{U}^{\text{coop}}(k + k^0;!) / [! + iD(k + k^0)^2] \hat{U}_1^c + \frac{1}{! + iD(k + k^0)^2 + i\frac{1}{\tau_{\text{topo}}}} \hat{U}_2^c + \quad ; \quad (4)$$

(see Fig. 11 and its caption for the definition of  $\hat{U}^{\text{coop}}(k + k^0;!)$ ). In section. IV, we will see that, at the critical point ( $m = 0$ ), these two contributions give rise to the same amplitude of the antiweak-localization (AWL) correction to the electric conductivity. When the finite topological mass is introduced, however, the Cooperon associated with the parity mode channel becomes inactive, since its backward scattering behaviour is truncated by the cutoff  $\frac{1}{\tau_{\text{topo}}}$ . Meanwhile, the Cooperon obtained from the charge mode channel remains active, even in the presence of finite  $m$ . As a result, the AWL correction

at the critical point becomes precisely halved, on introducing the finite topological mass (quantum correction doubling).

In terms of this novel behaviour of the parity diffusion mode and that of the corresponding A WL correction, we will argue in the section. V the possible microscopic mechanism of how the delocalized bulk-wavefunction emerges at the critical point, i.e.  $m = 0$ . To be more specific, we expect that the parity diffusion mode mentioned above generally becomes massless, when a system transits from the topological insulator side to the ordinary insulator side. Assuming that this is the case, we will attribute the emergence of the extended bulk wavefunction to the A WL correction obtained from this parity mode channel, i.e. the second term of eq. (4). For the systematic understanding, however, one generally needs to go beyond the theoretical approach employed in this paper. Several open issues will be also discussed in the section V.

A number of appendices describe other topics useful in understanding the main text in more detail. For clarity of the explanation, we have presented the results only in the case of chemical-potential type disorder in the text. The study in the presence of general T-symmetric disorders becomes more cumbersome. But the basic feature such as the phase diagram is expected to be same. In the appendix A, we will describe how the one-particle Green function at the zero-energy state behaves in the presence of these general T-invariant random potentials.

Our weak-localization calculation described in the section. IV is the controlled analysis, when it comes to the weakly disordered region,  $\lambda < \lambda_c$ . Namely, for this parameter region, one can confirm self-consistently the coupling constant  $l = k_F l = 1$  to be sufficiently small around  $\lambda = 0$  (see eq. (70)). For  $\lambda > \lambda_c$ , however, this coupling constant generally diverges toward  $\lambda = 0$ , only to make the weak localization calculation (and scB calculation) an uncontrolled analysis. Thus, as the complementary analysis for this strongly disordered region,  $\lambda > \lambda_c$ , we employed the mode-mode coupling analysis in the appendices. B-D. By taking into account the quantum interference effect due to the Cooperon terms, this theoretical framework gives us the gap equation for the diffusion constant. Main results in section. IV such as the quantum correction doubling are also supported by the analysis in the appendices. B-D.

## II. EFFECTIVE CONTINUUM MODEL AND DISORDER

### A. Effective continuum model

We consider a system with both T-symmetry and the spatial inversion (I)-symmetry. Under this symmetry requirement, Murakami et al. recently derived them in a minimal model for an arbitrary quantum critical point intervening the topological insulator and an ordinary insulator

on a quite general ground<sup>24,25</sup>. It turns out to be always described by the 3+1D Dirac fermion given as follows;

$$H_0 = \int d^3r \sum_{\mathbf{r}} \psi^\dagger(\mathbf{r}) \left[ \sum_{\alpha=1}^3 \hat{\alpha}_\alpha \partial_\alpha + m \hat{\alpha}_5 \right] \psi(\mathbf{r}); \quad (5)$$

where  $m$  corresponds to the topological mass term. Without loss of generality, one can regard the topological insulator phase to be  $m > 0$  and an ordinary insulator phase to be  $m < 0$  (see Fig. 1). To see that  $\psi$  actually endows this Dirac fermion with a mass, we note that following  $4 \times 4$  matrices are anticommuting with one another;

$$\begin{aligned} \hat{\alpha}_1 &= \hat{\sigma}_x, \hat{\alpha}_2 = \hat{\sigma}_y, \hat{\alpha}_3 = \hat{\sigma}_z, \hat{\alpha}_5 = \hat{\sigma}_0 \\ \hat{\beta}_1 &= \hat{\sigma}_0, \hat{\beta}_2 = \hat{\sigma}_x, \hat{\beta}_3 = \hat{\sigma}_y, \hat{\beta}_4 = \hat{\sigma}_z \end{aligned}$$

The matrices  $\hat{\alpha}$  and  $\hat{\beta}$  are Pauli matrices, representing the (generalized) sublattice index, and the spin index, respectively. In terms of these Pauli matrices, we will take the T operator as  $i\hat{\sigma}_y K$  with  $K$  being the complex conjugation. Meanwhile, the I operator will be taken as  $\hat{\alpha}_x$ . It follows from these conventions that  $\hat{\alpha}_{1,2,3,4}$  are T odd and I odd, while  $\hat{\alpha}_5$  is T even and I even (see table. I). Together with the property that  $i\hat{\sigma}_y$  is T odd and I odd, we can easily see that our Hamiltonian in the clean case is indeed T even and I even. This guarantees the Kramers degeneracy at each k-point, irrespectively of the topological mass  $m$ . We also note that eq. (5) is indeed the low-energy effective continuum Hamiltonian for various lattice models recently discussed in literatures<sup>15,19,20</sup>.

Dirac matrices			T	I
$\hat{\alpha}_0$	1	1	+	+
$\hat{\alpha}_1$	$\hat{\alpha}_y$	1		
$\hat{\alpha}_2$	$\hat{\alpha}_z$	$\hat{\sigma}_x$		
$\hat{\alpha}_3$	$\hat{\alpha}_z$	$\hat{\sigma}_y$		
$\hat{\alpha}_4$	$\hat{\alpha}_z$	$\hat{\sigma}_z$		
$\hat{\alpha}_5$	$\hat{\alpha}_x$	1	+	+

TABLE I: Dirac operators and their symmetries.

Generally speaking, we can enumerate all Hermitian matrices possible in this spin-sublattice space. Namely, using the commutator between these  $16$  Dirac matrices, we have other  $10$   $5C_2$  associated Dirac matrices;

$$\hat{\alpha}_{ij} = \frac{1}{2i} [\hat{\alpha}_i, \hat{\alpha}_j] = i\hat{\alpha}_i \hat{\alpha}_j; \quad (6)$$

We can further classify these 10 matrices into two classes; one is T invariant (even) matrices and the other is T odd. Since the  $16$  Dirac matrices are always even under I, these 10 associated Dirac matrices are by construction odd under I. Thus the symmetries of these 10 matrices can be summarized as in Table II.

10 matrices	T	I
$\hat{A}_{15}^z$	1	+
$\hat{A}_{25}^y$	$\hat{S}_x$	+
$\hat{A}_{35}^y$	$\hat{S}_y$	+
$\hat{A}_{45}^y$	$\hat{S}_z$	+
$\hat{A}_{12}^x$	$\hat{S}_x$	+
$\hat{A}_{13}^x$	$\hat{S}_y$	+
$\hat{A}_{14}^x$	$\hat{S}_z$	+
$\hat{A}_{23}^1$	$\hat{S}_x$	+
$\hat{A}_{34}^1$	$\hat{S}_y$	+
$\hat{A}_{42}^1$	$\hat{S}_z$	+

TABLE II: Dirac associated operators and their symmetries

Let us introduce T-symmetric "on-site type" random potentials as generally as possible;

$$H_{\text{imp}} = \sum_{\mathbf{r}} \sum_{\mathbf{r}'} v_0 \delta_{\mathbf{r}, \mathbf{r}'} + \sum_{\mathbf{r}} \sum_{\mathbf{r}'} v_5 \hat{A}_{j5}^{\mathbf{r}}(\mathbf{r}) \quad (7)$$

where all the 6 components of the vector  $\mathbf{v}(\mathbf{r})$  are real-valued functions of  $\mathbf{r}$ . Then, each single-particle eigenstate of  $H_0 + H_{\text{imp}}$  always has a Kramer's pair state;

$$\hat{H} \tilde{\psi}(\mathbf{r}) = \hat{I} \tilde{\psi}(\mathbf{r}) \quad (8)$$

Namely,  $\tilde{\psi}(\mathbf{r})$  and  $\hat{I} \tilde{\psi}(\mathbf{r})$  are degenerate and orthogonal to each other. Noting this, one can see that the retarded (advanced) Green function observes the following relation in each ensemble;

$$\hat{G}^{R(A)}(\mathbf{r}; \mathbf{r}^0; \omega) = \hat{I} \hat{S}_j \hat{G}^{R(A)}(\mathbf{r}^0; \mathbf{r}; \omega)^t \hat{I} \hat{S}_j \quad (9)$$

B. Disorder averages, spatial inversion symmetry, rotational symmetry and engineering dimension

As usual, we will take the quenched-average of these T-invariant in purities at the gaussian level;

$$\overline{P[\mathbf{v}]} = \frac{1}{N} \int \prod_{\mathbf{r}} d\mathbf{v}(\mathbf{r}) e^{-\sum_{\mathbf{r}} \mathbf{v}(\mathbf{r}) \cdot \mathbf{v}(\mathbf{r})} \quad (11)$$

with a proper normalization factor  $N$  and real-valued symmetric matrix  $\hat{A}$ . For simplicity, an "on-site type" correlation will be assumed;

$$\langle \hat{A}_{j5}^{\mathbf{r}}(\mathbf{r}) \hat{A}_{j5}^{\mathbf{r}^0}(\mathbf{r}^0) \rangle = \delta_{\mathbf{r}, \mathbf{r}^0} \quad (12)$$

We also suppose that the translation symmetry and the spatial inversion symmetry are recovered after these quenched averages;

$$\hat{G}^{R(A)}(\mathbf{r}; \mathbf{r}^0; \omega) = \hat{G}^{R(A)}(\mathbf{r} + \mathbf{b}; \mathbf{r}^0 + \mathbf{b}; \omega); \quad (13)$$

$$\hat{G}^{R(A)}(\mathbf{r}; \mathbf{r}^0; \omega) = \hat{A}_x \hat{I} \hat{G}^{R(A)}(\mathbf{r}; \mathbf{r}^0; \omega) \hat{A}_x \quad (14)$$

Then, the latter symmetry, i.e. eq. (14), prohibits any matrix elements between  $\hat{A}_{0,5}$  and  $\hat{A}_{j5}$  ( $j = 1, 2, 3, 4$ ) in the right hand side of eq. (12). Namely, the 6  $\times$  6 matrix  $\hat{A}$  in its right hand side takes the following form;

$$\hat{A} = \begin{pmatrix} \hat{A}_{00} & \hat{A}_{05} & 0 \\ \hat{A}_{50} & \hat{A}_{55} & 0 \\ 0 & 0 & \hat{A}_a \end{pmatrix} \quad (15)$$

with

$$\hat{A}_a = \begin{pmatrix} \hat{A}_{15} & \hat{A}_{14} \\ \hat{A}_{45} & \hat{A}_{44} \end{pmatrix} \quad (16)$$

This is because  $\hat{A}_{0,5}$  are even under  $\hat{I}$ , while  $\hat{A}_{j5}$  ( $j = 1, 2, 3, 4$ ) are odd. In order that the gaussian integral in eq. (10) converges, all the eigenvalues of  $\hat{A}$  have to be positive. Accordingly, the matrix elements described in eqs. (15-16) must obey the following inequalities;

$$\hat{A}_{00} > \hat{A}_{55} > 0; \quad \text{Tr} \hat{A}_a > 0; \quad (17)$$

We can study the effects of these general T-invariant "on-site type" random potentials, without any further assumptions. As will be partly shown in the Appendix A, however, such an analysis becomes very cumbersome and lengthy. Thus, we henceforth consider only the chemical potential type disorder  $\hat{A}_{00}$ , because it is expected to be dominant among various types of disorder. Those who are interested in the effects of other components such as  $\hat{A}_{05}$ ,  $\hat{A}_{55}$  and  $\hat{A}_a$  may consult the appendix A. In Appendix A we have studied the effect of the T-reversal invariant "on-site type" disorder on a general ground, focusing on the zero-energy wavefunction at the critical point.

Being translationally invariant as in eq. (13), the averaged Green functions can be readily Fourier-transformed by the use of the crystal momentum  $\mathbf{k}$ . The resulting Green functions can be expanded in terms of Dirac matrices and its associates;

$$\hat{G}^R(\mathbf{k}; \omega) = \sum_{j=0,5,1,2,3,4} \bar{F}_j(\mathbf{k}; \omega) \hat{A}_j \quad (18)$$

$\bar{F}_i(\mathbf{k}; \omega)$  stands for some complex-valued function of  $\mathbf{k}$  and  $\omega$ . In this momentum representation, T and I invariance, i.e. eq. (9) and eq.(14), read as follows;

$$\hat{A}_x \hat{I} \hat{G}^{R(A)}(\mathbf{k}; \omega) \hat{A}_x \hat{I} = \hat{G}^{R(A)}(\mathbf{k}; \omega); \quad (19)$$

$$\hat{I} \hat{S}_j \hat{G}^{R(A)}(\mathbf{k}; \omega) \hat{I} \hat{S}_j = \hat{G}^{R(A)t}(\mathbf{k}; \omega) \quad (20)$$

These two symmetries require that  $\bar{F}_{i=1; \quad}(\mathbf{k}; \quad)$  are odd functions of  $\mathbf{k}$ ,  $\bar{F}_{0,5}$  are even functions of  $\mathbf{k}$ , and also that  $\bar{F}_{ij} = 0$  for  $i \neq j$  and  $i, j = 1; \quad; 5$ . Namely, the retarded and advanced Green functions are given only in terms of the anti-commuting Dirac matrices;

$$\hat{G}^R(\mathbf{k}; \quad) = \bar{F}_0(\mathbf{k}; \quad) \hat{1} + \sum_{=1}^5 \bar{F}(\mathbf{k}; \quad) \wedge; \quad (21)$$

$$\hat{G}^A(\mathbf{k}; \quad) = \bar{F}_0(\mathbf{k}; \quad) \hat{1} + \sum_{=1}^5 \bar{F}(\mathbf{k}; \quad) \wedge; \quad (22)$$

In addition to the T-symmetry and I-symmetry, the pseudo-spin rotational symmetry is also recovered after the quenched average. This is because only the chemical-potential type disorder  $\epsilon_{00}$  is considered now. Specifically, the 1-point Green function after the quenched average respects the simultaneous rotations of the spatial coordinate and the pseudo-spin coordinate;

$$\hat{U}_n; \quad \hat{G}^{R(A)}(\mathbf{k}; \quad) \hat{U}_n^\dagger; \quad \hat{G}^{R(A)}(\mathbf{R}_n; \mathbf{k}; \quad); \quad (23)$$

$$\hat{U}_n; \quad e^{i\mathbf{R}_n \cdot \mathbf{k}} \wedge;$$

, and above run over 1;2 and 3.  $\mathbf{R}_n$  in the right hand side stands for the spatial rotation around the vector  $\mathbf{n}$  by the angle  $\theta$ . When combined with eqs. (19,20), this rotational symmetry further restricts the form of the Green functions. For example, the coefficient of  $\wedge_4$  should be an odd function of  $\mathbf{k}$  due to eq. (19), while it should be an even function of  $\mathbf{k}$  because of eq. (23). As such, Green functions cannot contain  $\wedge_4$ -component, under these two symmetry requirements. Moreover, eq. (23) by itself compels  $\bar{F}_{1,2,3}(\mathbf{k}; \quad)$  to be transformed as a vector under the rotation in the  $\mathbf{k}$ -space;

$$\bar{F}(\mathbf{k}; \quad) = c_1 \mathbf{k} + c_3 k^2 \mathbf{k} + \quad;$$

with  $= 1;2;3$ .

So far, we have imposed several generic symmetries such as T-symmetry and I-symmetry on the Green function after the quenched averaged. As a result of this, the Green function is given only in terms of the Dirac matrices. Since these 5 Dirac matrices are all anti-commuting with one another, the inverse of the Green function can be easily calculated,

$$\hat{G}^{R; \quad}(\mathbf{k}; \quad) = \bar{F}_0(\mathbf{k}; \quad) \hat{1} + \sum_{=1}^5 \bar{F}(\mathbf{k}; \quad) \wedge; \quad (25)$$

$$\bar{F}_0 = \frac{F_0}{F_0^2 - \sum_{=1}^5 F^2}; \quad \bar{F} = \frac{F}{F_0^2 - \sum_{=1}^5 F^2}; \quad (26)$$

Correspondingly, the inverse of the bare Green function is given as follows;

$$\hat{G}_0^{R; \quad}(\mathbf{k}; \quad) = (\epsilon + i) \hat{1} + \sum_{=1;2;3}^X \mathbf{k} \wedge + m \wedge_5$$

$$\sum_{=0; \quad; 5}^X f \wedge; \quad (27)$$

Based on these simplifications, we will derive in the next two sections the electronic property of the disordered single copy of 3 + 1 Dirac fermion described by eq. (5). Before finalizing this section, however, it would be appropriate to summarize the engineering dimension of the various quantities introduced in this section. Comparing the impurity Hamiltonian with the pure Hamiltonian, one can first see that

$$m; \mathbf{k}; \quad; f; F; v_i \quad [L^{-1}]; \quad \bar{F} \quad [L]; \quad (28)$$

where  $L$  denotes the dimension of a length. Out of this, we can further figure out the engineering dimension of  $j_m$ ;

$$j_m \quad [L]; \quad (29)$$

by requiring  $P[v]$  in eq. (11) to be dimensionless.

### III. SELF-CONSISTENT BORN APPROXIMATION

The self-consistent Born (scB) approximation simply equates the right hand sides of the following two;

$$\hat{G}^R(\mathbf{k}; \quad) = \hat{G}_0^{R; \quad} + \sum_{=1}^5 \hat{G}^{R; \quad}; \quad (30)$$

$$\hat{G}^R(\mathbf{k}; \quad) = \sum_{00} \int \frac{d^3 k^0}{Z} \hat{G}^R(\mathbf{k}^0; \quad)$$

$$= \sum_{00} \int \frac{d^3 k^0}{0 < \mathbf{k} \cdot \mathbf{k}} \bar{F}_0(\mathbf{k}^0; \quad) \wedge_0 + \bar{F}_5(\mathbf{k}^0; \quad) \wedge_5 \quad (31)$$

We have already omitted those terms proportional to  $\bar{F}_{1,2,3,4}(\mathbf{k}^0; \quad)$  in the integrand of eq. (31), since they are odd functions of  $\mathbf{k}^0$ . Comparing the coefficients of each matrix in eq. (30) and eq. (31), we can make the closed coupled equation for  $F_0$  and  $F_5$ ;

$$\sum_{00} \int \frac{d^3 k}{0 \leq \mathbf{k} \cdot \mathbf{k}} \frac{F_0}{F_0^2 - F_5^2 - k^2} = f_0 - F_0; \quad (32)$$

$$\sum_{00} \int \frac{d^3 k}{0 < \mathbf{k} \cdot \mathbf{k}} \frac{F_5}{F_0^2 - F_5^2 - k^2} = f_5 - F_5; \quad (33)$$

by the use of eq. (26). We have already used the following relations also;

$$F_{1,2,3} \quad f_{1,2,3} = k_{1,2,3}; \quad F_4 \quad f_4 = 0; \quad (34)$$

These integralequations in eqs. (32-33) clearly depend on the ultraviolet cut-off. Thus, rescaling the momentum by this cut-off, let us introduce the dimensionless quantities, instead of  $F$ ,  $f$ , and  $\epsilon_{00}$ . Eqs. (28-29) indicate that they should be rescaled in the following way;

$$F_{0,5} \rightarrow F_{0,5} \quad F_{0,5}^{-1}; \quad (35)$$

$$f_{0,5} \rightarrow f_{0,5} \quad f_{0,5}^{-1}; \quad (36)$$

$$\epsilon_{00} \rightarrow \epsilon_{00} \quad 2 \quad \epsilon_{00}; \quad (37)$$

The factor 2 in the definition of  $\tilde{G}$  is just for later convenience. In terms of these dimensionless quantities, the above coupled non-linear equations become;

$$(1 + \tilde{G})F_0 = f_0 \quad (38)$$

$$(1 - \tilde{G})F_5 = f_5 \quad (39)$$

where  $f_0$  and  $f_5$  in the right hand side are supposed to be also normalized by  $\tilde{G}$ .  $\tilde{G}$  used in the left hand side was also made dimensionless;

$$\tilde{G} = 2 \int_0^1 \frac{1}{(a + ib)^2} k^2 dk; \quad (40)$$

$$(a + ib)^2 = F_0^2 - F_5^2; \quad (41)$$

Eqs. (38-41) thus determine  $F_0$  and  $F_5$  as a function of

their bare values;  $f_0$  and  $f_5$ .  $F$  thus obtained should be by definition much smaller than the ultraviolet cut-off  $\Lambda$ ;

$$F \ll \Lambda; \quad (42)$$

This also leads to  $a, b \ll 1$ . In the followings, we will frequently take full advantage of their smallness, which is always self-consistently verified later (see below).

In the next subsection, we will present the solution of this coupled equation for general  $a$  and  $b$ . Before doing this, however, it would be appropriate to express the imaginary part and real part of  $\tilde{G}$  in terms of  $a$  and  $b$ , so that one can roughly estimate these two quantities in small  $a$  and  $b$ . The real part and the imaginary part of  $\tilde{G}$  read as follows;

$$\text{Re} \tilde{G} = 2 \frac{a}{2} \log \frac{(1 - a^2 + b^2)}{(1 + a)^2 + b^2} + b \text{Arctan} \frac{h_1 - a^i}{b} + \text{Arctan} \frac{h_1 + a^i}{b}; \quad (43)$$

$$\text{Im} \tilde{G} = \frac{b}{2} \log \frac{(1 - a^2 + b^2)}{(1 + a)^2 + b^2} - a \text{Arctan} \frac{h_1 - a^i}{b} + \text{Arctan} \frac{h_1 + a^i}{b}; \quad (44)$$

Observing these two, please notice that the final two terms in eq. (43-44), which are proportional to  $\text{Arctan}$ , are nothing but the pole contribution. Namely, the limit  $b \rightarrow 0$  reduces them a finite constant with its sign identical to that of  $b$ , e.g.

$$\text{Arctan} \frac{1 - a}{b} + \text{Arctan} \frac{1 + a}{b} \rightarrow \text{sgn}(b);$$

where one should also note that  $a, b \ll 1$ . Bearing these in mind, one can then evaluate the leading order of  $\text{Re} \tilde{G}$  and  $\text{Im} \tilde{G}$  with respect to small  $a$  and  $b$ ;

$$\text{Re} \tilde{G} = 2 + \mathcal{O}(a^2); \quad (45)$$

$$\text{Im} \tilde{G} = \text{sgn}(b) a + \mathcal{O}(ab); \quad (46)$$

Namely, the second member of eq. (45) and the first member of eq. (46) are nothing but the pole contributions mentioned above.

#### A. Solution for scB equations

##### 1. $m = 0$ case

For the warm-up, consider first the case with  $m = 0$ , i.e. the zero-energy state at the critical point. Equations (38-41) have three types of solutions;

$$(i) : F_0 = F_5 = 0; \quad (47)$$

$$(ii) : 1 + \tilde{G} = 0 \setminus F_5 = 0; \quad (48)$$

$$(iii) : 1 - \tilde{G} = 0 \setminus F_0 = 0; \quad (49)$$

Observing the estimates given in eqs. (45-46), please notice that type-(iii) solution cannot be satisfied for  $a > 0$  and  $a, b \ll 1$ . Thus, we will ignore this henceforth.

The type-(i) solution is always trivially satisfied. This solution indicates that the zero-energy state is not renormalized at all by the disorder,  $F_0 = f_0 = 0; F_5 = f_5 = 0$ . Thus, it describes the dimensionless zero-energy state.

The type-(ii) solution is a non-trivial solution, which turns out to describe the dispersive zero-energy state. To see this, let us begin with the first condition of eq. (48), i.e.  $1 + \tilde{G} = 0$ . The imaginary part of this gives  $\text{Im} \tilde{G} = 0$ , which is satisfied either when  $a = 0$  or when  $b = 0$  and  $|a| > 1$  (see Fig. 4). Since  $a, b \ll 1$  as noted earlier, the only physical solution satisfying  $\text{Im} \tilde{G} = 0$  is thus  $a = 0$ . The remaining condition,  $1 + \text{Re} \tilde{G} = 0$ , becomes then simple;

$$b \text{Arctan} b^{-1} = 1 - \frac{1}{2}; \quad (50)$$

Since  $F_5 = 0$  gives  $a + ib = F_0$ ,  $a$  and  $b$  thus obtained stand for the renormalized chemical potential  $\bar{\mu}$  and the inverse of the lifetime  $\tau^{-1}$ , respectively. Accordingly, the type-(ii) solution simply denotes that the zero-energy state acquires a finite lifetime, while its chemical potential is free from renormalizations;

$$\bar{\mu} = 0; \quad \tau^{-1} \text{Arctan} \tau^{-1} = 1 - \frac{1}{2}; \quad (51)$$

Namely, for  $\tau > \tau_c = \frac{1}{2}$ ,  $\tau^{-1}$  can take a finite value.

For a weak disorder region ( $\tau < \tau_c$ ), Eq. (51) cannot be satisfied for any  $\tau$ . Thus, the only solution therein is

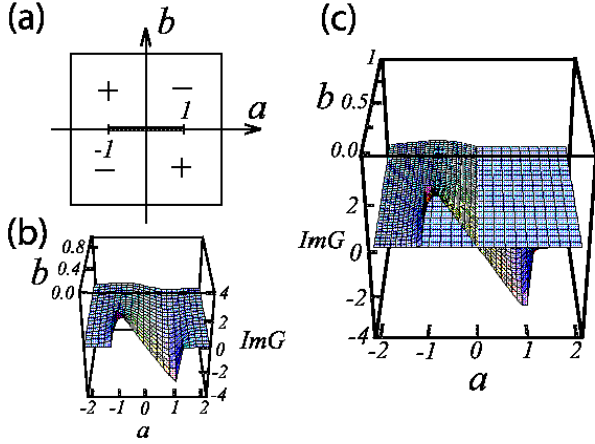


FIG. 4:  $\text{Im } G$  as a function of  $a$  and  $b$ . (a) The sign of  $\text{Im } G$ , which is an odd function both in  $a$  and in  $b$ . "+" stands for the sign of  $\text{Im } G$  at the 4 regions, i.e.  $a; b > 0$ ,  $a > 0 > b$ ,  $b > 0 > a$  and  $0 > a; b$ . The bold line which runs from  $(1; 0)$  to  $(0; 1)$  denotes a sort of the branch cut. Namely,  $\text{Im } G$  jumps from  $-2^{-2}a$  to  $+2^{-2}a$  (from  $b = +0$  to  $b = 0$ ). (b) A side view plot of  $\text{Im } G$  only for  $b > 0$ . (c)  $\text{Im } G = 0$  is satisfied either when  $a = 0$ , or when  $b = 0$  and  $a > 1$ .

the type-(i) trivial solution. On the other hand, both the type-(i) solution and type-(ii) solution become possible above this critical disorder strength ( $> c$ ). In the next three paragraphs, we will determine which solution is physically sensible for  $> c$ .

To do this, we will extend these two solutions into a small but finite region. Namely, by seeing how this chemical potential will be renormalized for each case, we will judge which solution is the physical one for  $> c$ . Recall first that  $F_5 = 0$  in either case. Thus,  $a$  and  $b$  correspond to  $^-$  and  $^1$  respectively, so that  $a$  and  $b$  should be an odd and an even function of the bare chemical potential respectively.

Bearing these in mind, let us extend the type-(i) solution into a small  $^-$ -region first. Namely, keeping the leading order in small  $^-$ , we can evaluate the real part of eq. (38);

$$(1 - 2^-)a + O(3^-) = ; \quad (52)$$

where we used  $a / O(1^-)$  and  $b / O(2^-)$ . Thus, the renormalized chemical potential is estimated up to  $O(1^-)$  as follows;

$$^- a = \frac{1}{2} + O(3^-); \quad (53)$$

while  $b$  will be determined up to  $O(2^-)$  from the imaginary part of eq. (38);

$$^1 b = \frac{1}{(1 - 2^-)^2} + O(4^-); \quad (54)$$

This solution indicates that the negative eigen-energy state and the positive eigen-energy state are inverted en-

ergetically for  $> c$ ;  $\text{sgn}^- = \text{sgn}^1$ . This is, however, clearly unphysical at least for small  $^-$ .

When the type-(ii) solution is extended into a small  $^-$ -region, a similar algebra gives us the following expression for the real part of eq. (38) up to  $O(1^-)$ ;

$$(1 - 2^-)a + 4^{-1} \text{Arctan}^- a = ; \quad (55)$$

In this equation, we have already made implicit those contributions proportional to  $O(3^-)$  and  $O(2^-)$  while keeping those proportional to  $O(1^-)$  explicit. Please also note that we have used  $a / O(1^-)$  and  $b = ^1 + O(2^-)$ . Namely, contrary to the type-(i) solution,  $b$  converges to a non-zero  $^1$  at the leading order in small  $^-$ . As a result of this, eq. (55) has acquired an additional  $O(1^-)$ -term, i.e.  $4^{-1} \text{Arctan}^- [ ] a$ , which was absent in eq. (52). This additional term makes the sign of  $^-$  to be same as that of  $^1$ . Namely, by the use of  $1 - 2^- = 2^{-1} \text{Arctan}^- + O(2^-)$ , eq. (55) leads us to;

$$(2^{-1} - 1)a + O(3^-) = ; \quad (56)$$

Out of this, one can evaluate the renormalized chemical potential up to  $O(1^-)$  as follows;

$$^- a = \frac{1}{2} + O(3^-); \quad (57)$$

whose sign is clearly same as that of the bare one for  $> c$ ;  $\text{sgn}^- = \text{sgn}^1$ . Observing these two distinct behaviors for the finite region, i.e. eq. (53) and eq. (57), we conclude that, for  $> c$ , the type-(ii) solution is the physically sensible solution, while the type-(i) solution is an unphysical one.

To summarize so far, the physical solutions obtained at  $m = 0$  are two-fold, depending on the disorder strength. When  $< c = 1/2$ , the type-(i) trivial solution is the only possible solution;

$$(i) : F_0 = F_5 = 0 \quad \text{for} \quad < c; \quad (58)$$

This means that the electronic state at the zero-energy is free from the disorder up to a certain critical disorder strength.

On the other hand, when its strength exceeds this critical value, i.e.  $> c$ , the type-(ii) solution should be adopted;

$$(ii) : F_0 = i^{-1}; F_5 = 0 \quad \text{for} \quad > c; \quad (59)$$

This solution means that the electronic state at the zero energy acquires a finite lifetime defined by eq. (51).

## 2. $m = 0$ and finite $m$ case

Let us introduce a finite topological mass  $m$  into eq. (58) and eq. (59) respectively, with the chemical potential being still zero. We will first argue that the



solution of eqs. (38-41) in the presence of the finite mass is uniquely determined for  $\alpha < \alpha_c$ . Such a solution reads;

$$F_0 = 0; F_5 = \bar{m}; \quad (60)$$

where  $\bar{m}$  is given as a function of the bare mass;

$$\bar{m} = 1 + 2 \sqrt{1 - \alpha} \arctan \sqrt{\frac{1}{1 - \alpha}} = m; \quad (61)$$

A typical behavior of  $\bar{m}$  as a function of the bare mass is depicted in Fig. 5 (b).

To see that eqs. (60-61) is the only possible solution for  $\alpha < \alpha_c$ , let us begin with the real part of  $1 + G$  appearing in eq. (38). In the case of  $\alpha < \alpha_c$ , it is always positive definite for any  $\alpha < 1$ . As such, we must take  $F_0$  to be zero, to satisfy eq. (38). This leads to  $F_5 = b$  via. Using this, consider next the imaginary part of eq. (39);

$$1 - \text{Re}G = a + \text{Im}G = b = 0; \quad (62)$$

Observing the leading-order estimates of  $\text{Re}G$  and  $\text{Im}G$ , i.e. eqs. (45-46), one can further see that eq. (62) uniquely leads to  $a = 0$ . The remaining condition, i.e. the real part of eq. (39), then becomes simple;

$$(1 - \text{Re}G) = b = 1 + 2 \sqrt{1 - \alpha} \arctan \sqrt{\frac{1}{1 - \alpha}} = b = m; \quad (63)$$

Now that  $(F_0; F_5) = (0; b)$ , this equation is nothing but eq. (61), when  $b$  replaced by  $\bar{m}$ .

Let us next consider the case of  $\alpha > \alpha_c$ . The solution of eqs. (38-41) in this case is two fold; we have a certain critical mass value  $m_c$ , which is given as a function of  $\alpha$ ;

$$m_c = 2 \sqrt{1 - \alpha}; \quad \sqrt{1 - \alpha} \arctan \sqrt{\frac{1}{1 - \alpha}} = \frac{1}{2}; \quad (63)$$

When the topological mass is less than this critical value ( $m < m_c$ ), the solution of eqs. (38-41) becomes;

$$F_0 = +i \frac{1}{\bar{m}^2}; F_5 = \bar{m} \frac{m}{2}; \quad (64)$$

where  $\bar{m}$  was already defined in eq. (63). On the other hand, when the topological mass exceeds this critical value ( $m > m_c$ ), the solution becomes eqs. (60-61) again.

To see that eq. (64) is the solution of eqs. (38-41) for  $\alpha > \alpha_c$  and  $m < m_c$ , take  $1 + G = 0$  first, so that eq. (38) is satisfied. By the use of the same arguments described above eq. (50), this immediately gives us  $(a; b) = (0; \frac{1}{2})$ , with  $\bar{m}$  being defined by eq. (61). Since  $1 - G = 2$ , eq. (39) leads to  $F_5 = m/2$ . Thus, using these two things, we obtain  $F_0$  out of eq. (41), which is nothing but eq. (64). When  $m$  exceeds  $m_c = 2 \sqrt{1 - \alpha}$ , eq. (64) becomes an unphysical solution in a similar way as the type-(i) solution in the previous subsection did for  $\alpha < \alpha_c$ ;

$$F_0 = +i \frac{1}{\bar{m}^2}; F_5 = \bar{m} \frac{m}{2};$$

Instead of this, it turns out that we should adopt the other solution for  $m > m_c$ , i.e. eqs. (60-61).

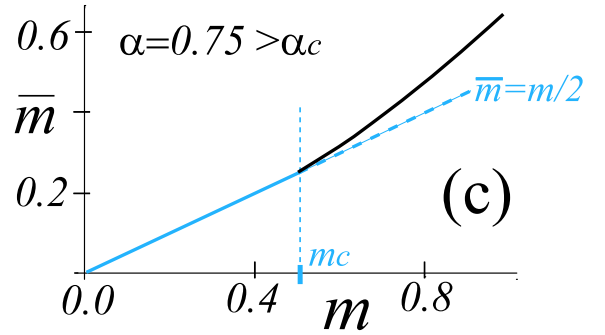
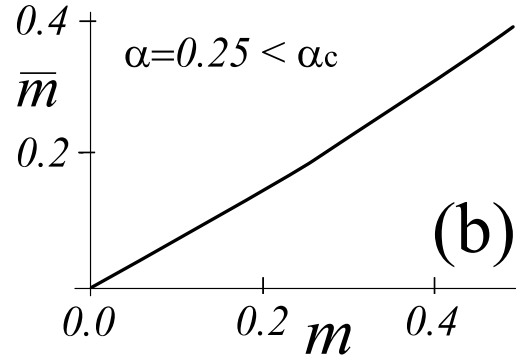
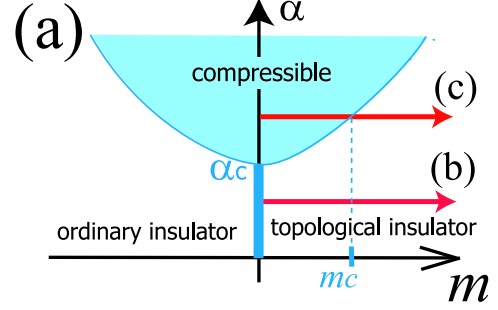


FIG. 5: (a); A schematic phase diagram at  $\alpha = 0$ . The white region corresponds to the incompressible phase, where no finite DOS exists at  $\alpha = 0$ . The blue region corresponds to the compressible states, where a finite DOS exists at  $\alpha = 0$ , i.e. eq. (64). (b) The renormalized mass  $\bar{m}$  as a function of the bare mass  $m$  for  $\alpha = 0.25 < \alpha_c$ . (c)  $\bar{m}$  as a function of  $m$  for  $\alpha = 0.75 > \alpha_c$ . There exists the critical value of the bare mass  $m$ , below which  $\bar{m} = m/2$ , and above which  $\bar{m}$  is determined by eq. (61). These two values coincide with each other precisely at  $m = m_c$ .

A typical behavior of  $\bar{m}$  in the case of  $\alpha > \alpha_c$  is depicted in Fig. 5 (c), where these two solutions, i.e. eq. (64) and eqs. (60-61), are indeed connected continuously at  $m = m_c$ . Since eq. (64) always supports a finite density of state (DOS), we can regard that the compressible phase extends over  $\alpha > \alpha_c$  and  $m < m_c$ . On the other hand, eqs. (60-61) do not support any finite DOS. As such, we can regard that an incompressible phase extends over  $\alpha < \alpha_c$  or  $m > m_c$  (Fig. 5(a)).

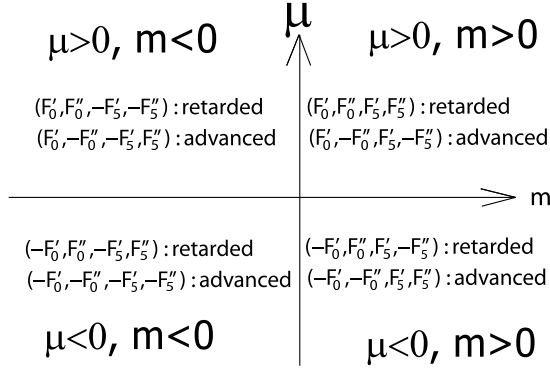


FIG. 6:  $F_0$  and  $F_5$  as a function of  $m$  and  $\mu$ .  $F_j^0$  and  $F_j^{\infty}$  are the real and imaginary part of a function  $F_j$ . At any parameter point, we generally have at least two solutions, which correspond to the retarded Green function and advanced one.

### 3. General $\mu$ and $m$ case

For finite  $\mu$  and  $m$ , both  $F_0$  and  $F_5$  are in general nonzero and we cannot solve eqs. (38-41) analytically. Accordingly, we have numerically solved the coupled equations with respect to  $a$  and  $b$ , so that  $F_0$  and  $F_5$  are derived in terms of  $\mu$  and  $m$ .

Before describing the numerical solution, let us first argue about the generic features of such solutions. Notice first that  $\text{Re}G$  is an even function of both  $a$  and  $b$ , while  $\text{Im}G$  is an odd function of both  $a$  and  $b$ . Thus the following two should be degenerate at any given  $\mu$  and  $m$  as the solutions of eqs. (38-41);

$$(F_0^0; F_0^{\infty}; F_5^0; F_5^{\infty}); (F_0^0; -F_0^{\infty}; F_5^0; -F_5^{\infty}); \quad (65)$$

where  $F_j^0$  and  $F_j^{\infty}$  are the real and imaginary part of  $F_j$ . Namely, these two solutions correspond to the retarded Green function and advanced one respectively.

The above two solutions at given  $m$  and  $\mu$  can be further extended into the other 3 quadrants, i.e.  $(-m; \mu)$ ,  $(m; -\mu)$  and  $(-m; -\mu)$ ;

$$\begin{aligned} & (F_0^0; -F_0^{\infty}; F_5^0; -F_5^{\infty})_{jm}; \\ & = (F_0^0; F_0^{\infty}; F_5^0; F_5^{\infty})_{j-m}; \\ & = (-F_0^0; F_0^{\infty}; F_5^0; F_5^{\infty})_{jm}; \\ & = (-F_0^0; -F_0^{\infty}; F_5^0; F_5^{\infty})_{j-m}; \end{aligned}$$

where the upper sign corresponds to the retarded function for any of these four regions by construction (Fig. 6). Observing this, please notice that both  $F_5^0$  and  $F_5^{\infty}$  vanish at  $m = 0$ , which is indeed the case with Sec.III-A1. Similarly, one can also see that  $F_0^0$  and  $F_0^{\infty}$  should vanish at  $\mu = 0$  for any  $m$ . Both eqs. (60-61) and eq. (64) actually observe this.

These considerations are also consistent with the numerical solution. In Fig. 7 and 8, we demonstrated numerically how  $F_0$  and  $F_5$  behave as a function of  $\mu$  and  $m$  (only for the first quadrant,  $m > 0$  and  $\mu > 0$ ), at

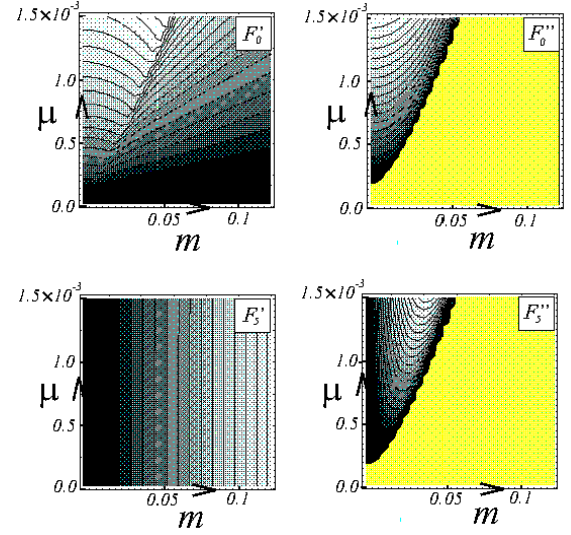


FIG. 7:  $\mu = 0.48$ ; (a): The contour plot of  $F_0^0$  as a function of  $\mu > 0$  and  $m > 0$ . The value of  $F_0^0$  decreases toward the dark region, and becomes zero at  $\mu = 0$ . The contour interval is  $1.2 \times 10^{-3}$ . (b): The contour plot of  $F_0^{\infty}$ . The value of  $F_0^{\infty}$  decreases toward the darker region, and becomes zero at the yellow region. The contour interval is  $0.6 \times 10^{-3}$ . (c): The contour plot of  $F_5^0$ .  $F_5^0$  decreases toward the darker region, and becomes zero at  $m = 0$ . The contour interval is  $4.0 \times 10^{-3}$ . (d): The contour plot of  $F_5^{\infty}$ .  $F_5^{\infty}$  increases toward the darker region and becomes zero at  $\mu = 0, m = 0$  and the yellow region. The contour interval is  $1.2 \times 10^{-5}$ .

specific values of  $\mu$ . Fig. 7 is for  $\mu < \mu_c$ , while Fig. 8 is for  $\mu > \mu_c$ . In the limit of  $\mu \rightarrow 0$ ,  $F_0$  and  $F_5$  in these two figures continuously connects with the two analytic solutions previously derived, i.e. eq. (60-61) and eq. (64) respectively.

We have also checked that, whenever  $F_0^{\infty} = F_5^{\infty} = 0$ ,  $F_5^0$  is always greater than  $F_0^0$ , i.e.  $a^2 - b^2 < 0$ . As such, the spectral function is identically zero, provided that both  $F_0^0$  and  $F_5^0$  vanish. Such a phase should be regarded as an incompressible phase having no bound states. On the one hand, when either  $F_0^{\infty}$  or  $F_5^{\infty}$  is finite, the spectral weight is finite and such a phase is compressible.

By seeing whether  $F_0^{\infty}$  and  $F_5^{\infty}$  totally vanishes or not, we have determined the phase diagram in the  $(m, \mu)$ -space. The phase boundaries between the compressible phase and the incompressible phase thus obtained are schematically drawn in Fig. 9, while accurately specified in Fig. 10. For  $\mu > \mu_c$ , we have a finite critical mass value, i.e.  $m_c$ , below which a compressible phase extends even at  $\mu = 0$  (Fig. 9(c) and Fig. 10(e,f)). This critical value goes to zero, when  $\mu$  goes to  $\mu_c$  from above (Fig. 10(d)). For  $\mu < \mu_c$ , we have a compressible region not in the  $\mu = 0$  region anymore, but still in the nonzero  $\mu$  region (Fig. 9(b) and Fig. 10(a-c)). The slope of the

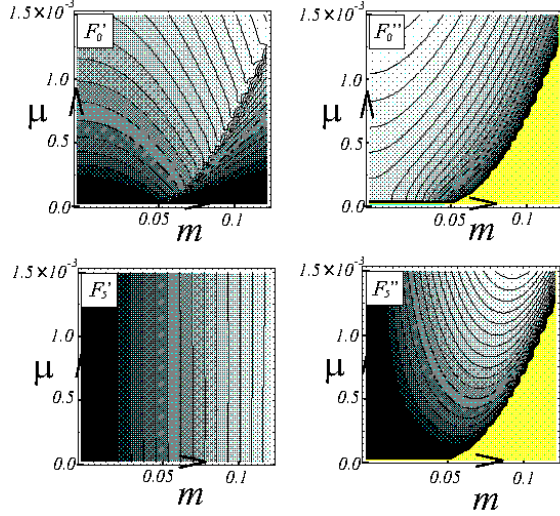


FIG. 8:  $\alpha = 0.52$ ; (a): The contour plot of  $F_0^0$  as a function of  $\mu > 0$  and  $m > 0$ . The value of  $F_0^0$  decreases toward the dark region, and becomes zero at  $\mu = 0$ . The contour interval is  $1.8 \times 10^{-3}$ . (b): The contour plot of  $F_0^0$ . The value of  $F_0^0$  decreases toward the darker region, and becomes zero at the yellow region. The contour interval is  $1.8 \times 10^{-3}$ . (c): The contour plot of  $F_5^0$ .  $F_5^0$  decreases toward the darker region, and becomes zero at  $m = 0$ . The contour interval is  $4.0 \times 10^{-3}$ . (d): The contour plot of  $F_5^0$ .  $F_5^0$  increases toward the darker region and becomes zero at  $\mu = 0, m = 0$  and the yellow region. The contour interval is  $3.0 \times 10^{-5}$ .

phase boundary in  $\alpha < \alpha_c$  given as follows;

$$\frac{d\alpha_c}{dm} \bigg|_{\alpha_c = m_c = 0} = \frac{1}{1+2} \frac{2}{2};$$

increases when the disorder strength decreases (Fig. 10 (a-c)).

#### IV. DIFFUSION AND QUANTUM CONDUCTIVITY CORRECTION

In the previous section, we have derived the 1-point Green function within the self-consistent Born approximation. In the 3-d parameter space spanned by  $\mu$ ,  $m$  and  $\alpha$ , we have observed that the topological insulator and an ordinary insulator are always intervened by the compressible phase (see the blue region in Fig. 9). The topological insulator supports a single  $2+1$  surface massless Dirac fermion on each boundary, while an ordinary insulator does not. As such, we expect that this intervening phase is composed by those wavefunctions which extend over an entire bulk (see section I for its reason).

As the first step to understand the nature of this compressible phase especially for  $\alpha < \alpha_c$ , we will calculate the series sum of the ladder-type diagram  $\hat{\chi}^d(q; !)$  (see Fig. 11 (a)), only to see that the diffusion thus obtained

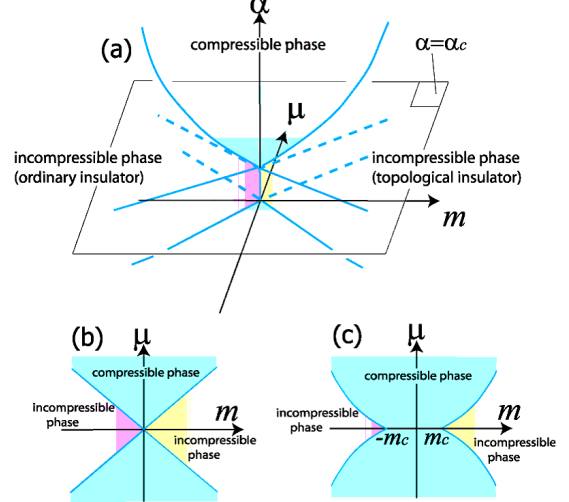


FIG. 9: (a) A schematic phase diagram in the  $\mu$ - $m$  space. Either  $F_0^0$  or  $F_5^0$  always remains finite in the compressible phase (blue), while both of them become zero at the remaining parameter region (incompressible phase), which is further divided into an ordinary insulator (red) and the topological insulator (yellow). (b) A schematic phase diagram in  $\mu$ - $m$  plane for  $\alpha < \alpha_c$ , and (c) that for  $\alpha > \alpha_c$ . These correspond to the numerical results shown in Fig. 10.

consists of two quasi-degenerate low-energy modes;

$$\hat{\chi}^d(q; !)/ \frac{1}{! + iD q^2} \hat{\chi}_1^d + \frac{1}{! + iD q^2 + i \frac{1}{\tau_{\text{topo}}}} \hat{\chi}_2^d + \quad (66)$$

with  $\frac{1}{\tau_{\text{topo}}} / m^2$ . The information of the charge diffusion is solely encoded into the first term, which thus always has the diffusion pole structure. On the other hand, the second term becomes massless only at  $m = 0$  (but generic  $\alpha$ ), while it suffers from the finite infrared cutoff  $\frac{1}{\tau_{\text{topo}}}$  for the finite  $m$  case. We will explicitly see that the second term is actually associated with the parity degree of freedom, which, at  $m = 0$ , becomes a conserved quantity of our effective continuum model, i.e. eq. (5).

When the hole line of  $\hat{\chi}^d(q; !)$  is time-reversed, these two-mode features are translated into the backward scattering channel associated with the "fan"-type diagrams  $\hat{U}^{\text{coop}}(k + k^0; !)$  (see Fig. 11 (b)). Namely, for small  $!$  and  $k + k^0$ , it is also dominated by two quasi-degenerate dominant contributions;

$$\hat{U}^{\text{coop}}(k + k^0; !)/ \frac{1}{! + iD (k + k^0)^2} \hat{U}_1^c + \frac{1}{! + iD (k + k^0)^2 + i \frac{1}{\tau_{\text{topo}}}} \hat{U}_2^c + \quad : \quad (67)$$

One is obtained from the charge mode channel, i.e.  $\hat{\chi}_1^d$ , with its hole-line time-reversed, while the other is from the parity mode channel,  $\hat{\chi}_2^d$ . In this section, we will further see that both of these two give rise to the same amplitude of the antiweak-localization (AWL) correction to

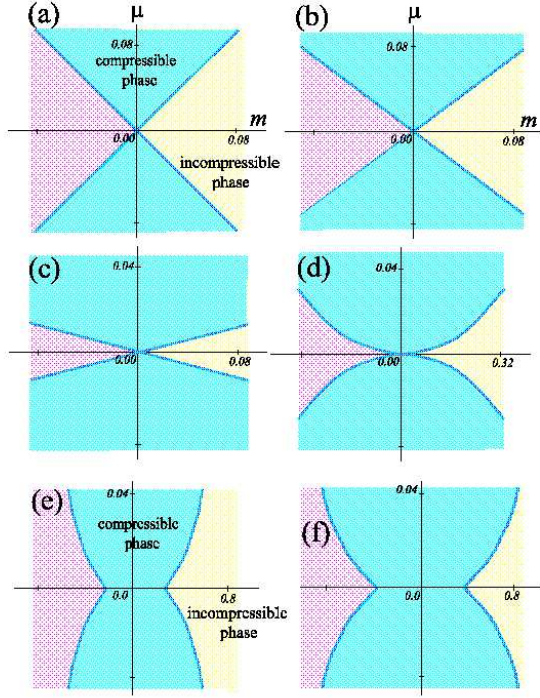
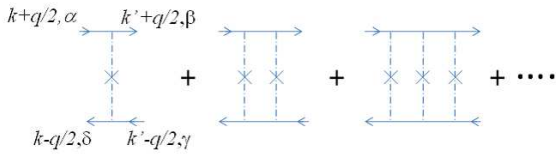


FIG. 10: Phase boundaries between the compressible phase and the incompressible (gapped) phase, in the  $m$  plane, at several values of  $c$ . (a)  $c = 0.0$ , (b)  $c = 0.1$ , (c)  $c = 0.4$ , (d)  $c = 0.5$ , (e)  $c = 0.6$ , (f)  $c = 0.7$ .

$$(a) \alpha \Gamma_{\alpha\beta,\gamma\delta}^d(q, \omega) =$$



$$(b) U_{\alpha\beta,\gamma\delta}^{\text{coop}}(k+k', \omega) =$$

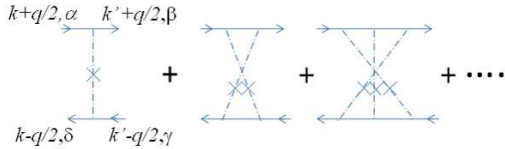


FIG. 11: (a) A series sum of the ladder-type diagrams  $\alpha \Gamma_{\alpha\beta,\gamma\delta}^d(q; !)$ , (b) A series sum of the "fan"-type diagrams  $U_{\alpha\beta,\gamma\delta}^{\text{coop}}(k+k'; !)$   $\hat{f} \hat{f} \hat{s}_y g_{-1}^{\wedge d};_{-1,1}(k+k^0; !)$   $\hat{f} \hat{s}_y g_{-1}$  :

the electric conductivity at  $m = 0$ . In the presence of the finite topological mass  $m$ , however, the second term in eq. (67) becomes less dominant, because of the finite infrared cut-off  $\frac{1}{\text{topo}}$ . Namely, half of the A WL correction becomes ineffective on increasing  $m$  ("quantum correction doubling").

Using these knowledges obtained in this section, we will propose in the next section the possible microscopic mechanism of how the bulk-critical region emerges between the topological insulator and an ordinary insulator.

This section is organized as follows. In Sec. IV-A, we will sum up the entire ladder-type diagram in the particle-hole channel, using the 1-point Green function obtained in the self-consistent Born calculation;

$$\hat{G}^{R; -1}(k; ; m) = F_0 \hat{1} - k^{\wedge} + F_5^{\wedge} s; \quad (68)$$

$$\hat{G}^{A; -1}(k; ; m) = F_0 \hat{1} - k^{\wedge} + F_5^{\wedge} s; \quad (69)$$

with  $F_0 = i^{-1}$  and  $F_5 / m$ . Such a summation should contain those contributions which diverge at  $! = 0$  and  $q = 0$ . We will identify this diverging contribution in the section IV-B, only to see that  $\hat{\Gamma}_d^d(q; !)$  contain two quasi-degenerate dominant contributions, as in eq. (66). Explicit expressions for  $\hat{\Gamma}_1^d$ ,  $\hat{\Gamma}_2^d$  and  $\frac{1}{\text{topo}}$  will be therefore given here. By calculating the parity-density correlation function, we will show in the section. IV-C that  $\hat{\Gamma}_2^d$  solely participates in the parity diffusion mode. Finally, the quantum conductivity corrections arising from these two terms are calculated in section. IV-D, based on the Kubo formula.

Comparing eqs. (53-54) with eqs. (57,59), notice also that the weak-localization (WL) calculation in this section becomes a controlled analysis only for the weak disorder region,  $c < c_c$ . Namely, the renormalized chemical potential and the lifetime  $\tau^{-1}$  determined in section. III guarantee a sufficiently small  $! = \tau^{-1}$  around  $! = 0$  only for this weak disorder region;

$$= \frac{1}{c} \frac{(c_c - c)^2}{2} \frac{1}{c} + 0 \quad \text{for } c < c_c: \quad (70)$$

For the strong disorder region, however,  $! = \tau^{-1}$  readily diverges around the zero energy region;

$$= \frac{c}{2} + 0^{-3} \quad \text{for } c > c_c: \quad (71)$$

Thus, the NCA approximation employed in section. III and the corresponding WL calculation described below acquire the small coupling constant  $\frac{1}{c}$ , only for  $c < c_c$ , but, for  $c > c_c$ , they generally don't. Bearing in mind especially this strong disorder region, we will demonstrate in the appendix. B the mode-mode coupling calculation, which is complementary to the weak-localization studies described in this section. Without resorting to the Kubo formula, this theoretical framework gives us the gap equation for the diffusion constant, taking into account the interference effects due to the Cooperon term.





After lengthy algebra, one can express its 12 coefficients  $f_j$  in terms of those of eq. (75) as follows;

$$\begin{array}{ccccccc} 2 & 3 & 2 & & 3 & & \\ 6 & 0 & 7 & & 6 & 3a_4 & a_4 & 3a_4 & a_4 & 7 \\ 1 & 1 & 1 & & 1 & a_1 & 3a_1 & a_1 & 3a_1 & 1 \\ 2 & 1 & 1 & & 1 & 3a_3 & a_3 & 3a_3 & a_3 & 1 \\ 3 & 1 & 1 & & 1 & 3a_3 & a_3 & 3a_3 & a_3 & 1 \\ 4 & 1 & 1 & & 1 & 3a_4 & a_4 & 3a_4 & a_4 & 1 \\ 5 & 1 & 1 & & 1 & a_4 & a_4 & a_4 & a_4 & 1 \\ 6 & 1 & 1 & & 1 & 3a_1 & 3a_1 & 3a_1 & 3a_1 & 1 \\ 7 & 1 & 1 & & 1 & a_1 & 3a_1 & a_1 & 3a_1 & 1 \\ 8 & 1 & 1 & & 1 & a_3 & a_3 & a_3 & a_3 & 1 \\ 9 & 1 & 1 & & 1 & a_3 & a_3 & a_3 & a_3 & 1 \\ 10 & 1 & 1 & & 1 & a_4 & a_4 & a_4 & a_4 & 1 \end{array} \quad \begin{array}{c} 1 \\ 8 \end{array} \quad \begin{array}{c} f_1 \\ f_3 \\ f_2 \\ f_4 \end{array} \quad (84)$$

$$11 \quad 3a_1^3 (f_4^{-1} + f_1^{-1}) f_1 f_2 = f_3 + f_4 ; \quad (85)$$

where  $a_{04}$ ,  $a_4$ ,  $a_{23}$ ,  $a_3$  and  $f_{1,2,3,4}$  are defined in terms of  $a_0$ ,  $a_1$ , and  $a$

$$a_3 = a_2 + a_3 ; a_4 = a_0 + a_4 ; \quad (86)$$

$$a_{23} = a_2 + a_3 ; a_{04} = a_0 + a_4 ; \quad (87)$$

$$f_1 = \frac{1}{a_1^2 + (a_4 + a_{23})(a_4 + a_{23})} ; \quad (88)$$

$$f_2 = \frac{1}{a_1^2 + (a_4 + a_{23})(a_0 + a_{23})} ; \quad (89)$$

$$f_3 = \frac{1}{9a_1^2 + (a_4 + a_{23})(a_4 + a_{23})} ; \quad (90)$$

$$f_4 = \frac{1}{9a_1^2 + (a_4 + a_{23})(a_0 + a_{23})} ; \quad (91)$$

#### B. Identification of the dispersion pole

Using eqs. (68-69), we have summed up the ladder-type diagram in the particle-hole channel, only to obtain eq. (82). The coefficients  $f_j$  appearing in eq. (82) are expressed in terms of  $F_0$  and  $F_5$ , by way of eqs. (84-91) and eq. (78). When the self-consistent Born (scB) solution is used for  $F_0$  and  $F_5$ , at least one of these  $f_j$  is expected to have a dispersion pole structure. On the one hand, none of  $a_j$  defined in eq. (78) does not diverge at  $! = 0$ . As such, some of  $f_j^{-1}$  should be zero at  $! = 0$ . In this subsection, we will identify which  $f_j$  diverges at small  $!$ . This also determines the asymptotic tensor-form of the diuson in the small  $!$  limit.

To do this, let us first start from the self-consistent Born equations of  $F_0$  and  $F_5$ , i.e. eqs. (38-41). Obviously, begin with the following two;

$$(F_0 - F_5) \sum_k \frac{(F_0 + F_5)}{k^2 (F_0^2 - F_5^2)} = m + i ; \quad (92)$$

$$(F_0 + F_5) \sum_k \frac{(F_0 - F_5)}{k^2 (F_0^2 - F_5^2)} = +m + i ; \quad (93)$$

Then, subtracting eqs. (92,93) by their complex conjugates respectively, we can readily obtain

$$\begin{array}{ccccccc} a_{04} & a_3 & 3a_1 & & F_0^0 & F_5^0 & \\ & 3a_1 & a_{04} + a_{23} & & F_0^0 + F_5^0 & & \end{array} = \begin{array}{ccccccc} \# & \# & \# & \# & \# & \# & \# \end{array} \quad (94)$$

where eq. (87) and eq. (78) were used. This equation indicates that the determinant of the  $2 \times 2$  matrix in the left hand side should be zero, provided that either  $F_0^0$  or  $F_5^0$  is non-zero. Any compressible phase having a finite density of state supports  $F_0^0 + F_5^0 \neq 0$ . As such, any scB solution in the compressible phase always guarantees the following identity;

$$9a_1^2 - a_4^2 + a_{23}^2 = 0 ; \quad (95)$$

Since  $a_1$  defined in eq. (78) is negative definite at  $! = 0$ , more accurately, eq. (95) should be replaced by;

$$3a_1 = 0 = \frac{q}{a_{04}^2 - a_{23}^2} ; \quad (96)$$

Observing eq. (91), notice that this is actually identical to the following,

$$f_4^{-1} = 0 ; \quad (97)$$

Namely,  $f_4$  carries the dispersion pole.

$f_1$ ,  $f_2$  and  $f_3$  generally cannot have any pole structure for the small  $!$  region. To see this explicitly, note first that, when generalized into the finite  $q$  case,  $f_4$  takes the following asymptotic form ;

$$f_4(!)' = \frac{1}{a_0} \frac{1}{i!} \quad (98)$$

In the right hand side, we have replaced  $i!$  by  $i! - D_0 q^2$  with the bare dispersion constant  $D_0$ . By retaining the subleading contribution in small  $q$  appearing in eq. (73), one can explicitly calculate its leading order expression in the large  $!$  limit;

$$D_0 = \frac{1}{6} \frac{c}{c +} ; \quad (99)$$

which is positive definite for  $c < c_c$ . Similarly, we can obtain the asymptotic form of  $f_1$ ,  $f_2$  and  $f_3$  at  $! \rightarrow 0$ ;

$$f_1' = \frac{1}{a_0} \frac{1}{i!} \frac{1}{D_1 q^2} ; \quad (100)$$

$$f_2' = \frac{1}{a_0} \frac{1}{i!} \frac{1}{D_2 q^2} ; \quad (101)$$

$$f_3' = \frac{1}{a_0} \frac{1}{i!} \frac{1}{D q^2} ; \quad (102)$$

$f_1^{-1}$  and  $f_2^{-1}$  above are positive definite;

$$\begin{array}{c} f_1^{-1} \\ f_2^{-1} \end{array} + \frac{1}{D_{topo}} > 0 ; \quad (103)$$

while  $\frac{1}{\text{topo}}$  being positive semi-definite;

$$\frac{1}{\text{topo}} = \frac{4(a_0 a_4 + a_2 a_3)}{a_0} \quad \text{for } j! = 0 \quad (104)$$

The two inequalities in eq. (103) and eq. (104) are indeed supported by eq. (79) and eqs. (79-80) respectively. These expressions indicate that  $f_1, f_2$  and  $f_3$  always experience the infrared cutoff for the low-energy and long wavelength region.

Comparing eq. (104) with eq. (81), notice also that  $\frac{1}{\text{topo}}$  reduces to zero in the massless case,  $\frac{1}{\text{topo}} / m^2$ , since  $a_2, a_3$  and  $a_4$  being zero. As such,  $f_3$  acquires a semi-discrete pole as  $f_4$  does in the absence of the topological mass. Meanwhile  $f_1$  and  $f_2$  always suffer from the (relatively large) finite infrared cutoff  $\frac{1}{2}$ , irrespectively of the topological mass term. Thus, we will retain in eq. (84) only those terms proportional to  $f_3$  and  $f_4$ . Based on the same spirit, we will also replace eq. (85) by its leading order contribution in small  $q$  and  $q$ ;

$$f_3 \approx \frac{3a_1}{8} f_3 + f_4; \quad (105)$$

and use the following asymptotic expressions for  $f_0$ ;

$$\begin{aligned} f_0 &\approx \frac{a_0}{8} f_3 + \frac{a_0}{8} f_4 \\ f_1 &\approx \frac{3a_1}{8} f_3 + \frac{3a_1}{8} f_4 \\ f_2 &\approx \frac{a_2}{8} f_3 + \frac{a_2}{8} f_4 \end{aligned}$$

With these equations, the asymptotic form of the diffusion in small  $q$  will be derived out of eq. (82). It consists of the two quasi-degenerate dominant contributions;

$$\hat{\chi}^d(q;!) \approx \frac{f_4}{8} \hat{\chi}_1^d + \frac{f_3}{8} \hat{\chi}_2^d; \quad (106)$$

where the two  $q$ -free tensors are given as follows;

$$\hat{\chi}_1^d = \frac{1}{4} \begin{pmatrix} \hat{I} + \hat{I}_4 & \hat{I} + \hat{S}_1 \\ \hat{I} + \hat{I}_4 & \hat{I} + \hat{S}_2 \\ \hat{I}_2 + \hat{I}_3 & \hat{I} + \hat{S}_1 \end{pmatrix}; \quad (107)$$

$$\hat{\chi}_2^d = \frac{1}{4} \begin{pmatrix} \hat{I} & \hat{I}_4 & \hat{I} + \hat{S}_1 \\ \hat{I} & \hat{I}_4 & \hat{I} + \hat{S}_2 \\ \hat{I}_2 & \hat{I}_3 & \hat{I} + \hat{S}_1 \end{pmatrix}; \quad (108)$$

## C. parity diffusion mode

To capture the physical meanings of the two members in eq. (106), notice first that, in the absence of the topological mass  $m$ , our hamiltonian, i.e. eq. (5) with the chemical-potential type disorder, becomes invariant under the following  $U(1)$  transformation;

$$e^{i \int d^3x \psi(x) \hat{A}_5(x)} \hat{H} e^{i \int d^3x \psi(x) \hat{A}_5(x)} = \hat{H}; \quad (109)$$

irrespectively of the strength of the disorder. As a result, each ensemble at  $m = 0$  acquires another conserved charge,  $\int d^3x \psi(x) \hat{A}_5(x)$ , which is the parity density degree of freedom (see Table II). Observing this  $U(1)$  symmetry, we can then expect that the diffusion  $\hat{\chi}^d(q;!)$  calculated above should consist of two diffusive modes at  $m = 0$ : One describes the usual charge diffusion and the other is for the diffusion of this parity density. These two physical modes actually correspond to the first term and the second term in eq. (106) respectively. In fact, the parity density becomes non-conserved in the presence of  $m$ , which is consistent with the finite infrared cutoff  $\frac{1}{\text{topo}} / m^2$  appearing only in  $f_3$  (see eqs. (102,98)).

To uphold this consideration more directly, one can also calculate the density correlation function and parity density correlation function at  $m = 0$ ;

$$\begin{aligned} \chi_0(q;!) &= \int d^3x \langle \psi(x) \psi(x+k) \rangle; \\ \chi_{45}^0(q;!) &= \int d^3x \langle \psi(x) \hat{A}_5(x+k) \rangle; \end{aligned}$$

where  $\hat{\chi}(k; k^0; q;!)$  stands for the response function (see eq. (B2) for its definition). By noting that this response function for small  $q$  and  $!$  is dominated by the diffusion;

$$\hat{\chi}^d(q;!) \approx \frac{1}{2} \hat{G}_1^R(k_+;!) \hat{G}_1^A(k_-;) + \frac{1}{2} \hat{G}_1^R(k_+^0;!) \hat{G}_1^A(k_-^0;); \quad (110)$$

one can explicitly see that the two terms appearing in eq. (106) actually contribute the density correlation and parity density correlation separately;

$$\chi_0(q;!); \chi_{45}^0(q;!) \approx \frac{8ia_0}{8} f_4; f_3; \quad (111)$$

## D. Cooperon and the quantum conductivity correction

When the hole lines being time-reversed, eq. (106) will be transcribed into the two quasi-degenerate dominant contributions to the series sum of the "fan"-type diagrams (see Fig. 11(b));

$$\hat{U}^{\text{coop}}(k + k^0;!) = \frac{1}{8} f_4 \hat{U}_1^c + f_3 \hat{U}_2^c; \quad (112)$$

where the  $\hat{U}_{1;2}^c$  are derived out of eqs. (107-108) respectively;

$$\hat{U}_1^c = \frac{1}{8} \left( \hat{f}_4 + \hat{f}_3 \right) \hat{U}_{1;2}^c; \quad \hat{U}_2^c = \frac{1}{8} \left( \hat{f}_4 - \hat{f}_3 \right) \hat{U}_{1;2}^c; \quad (113)$$

$$\hat{U}_{1;2}^c = \frac{1}{8} \left( \hat{f}_4 + \hat{f}_3 \right) \hat{U}_{1;2}^c; \quad \hat{U}_{1;2}^c = \frac{1}{8} \left( \hat{f}_4 - \hat{f}_3 \right) \hat{U}_{1;2}^c; \quad (114)$$

Substituting these two Cooperon terms into the current-current correlation function, we can explicitly show that the two members in eq. (112) lead the same magnitude of the anti-weak-localization (AWL) behaviour at the critical point ( $m = 0$ );

$$\begin{aligned} & \frac{1}{8} \left( \hat{f}_4 + \hat{f}_3 \right) \hat{U}_{1;2}^c; \quad \frac{1}{8} \left( \hat{f}_4 - \hat{f}_3 \right) \hat{U}_{1;2}^c; \\ & = \frac{1}{8} \left( \hat{f}_4 + \hat{f}_3 \right) \hat{U}_{1;2}^c; \quad \frac{1}{8} \left( \hat{f}_4 - \hat{f}_3 \right) \hat{U}_{1;2}^c; \\ & = \frac{1}{8} \left( \hat{f}_4 + \hat{f}_3 \right) \hat{U}_{1;2}^c; \quad \frac{1}{8} \left( \hat{f}_4 - \hat{f}_3 \right) \hat{U}_{1;2}^c; \\ & = c \left( 1 - \frac{1}{L} \right) \end{aligned} \quad (115)$$

with  $c = 16 \left( 1 - \frac{1}{L} \right)$  being positive definite. (we used  $a_2 = a_3 = a_4 = 0$  and  $3a_1 = a_0$  in eqs. (113-114)). When the finite topological mass is introduced, however, the second member of eq. (112) becomes suppressed, since the infrared divergence of  $f_3$  becomes truncated by finite  $\frac{1}{\text{topo}}$ . As a result, one half of the AWL correction becomes ineffective in the presence of finite ( $\backslash$ quantum correction doubling").

## V. DISCUSSION

### A. Summary of our findings

In this paper, we have studied the effects of the time-reversal invariant disorder on the quantum spin Hall system<sup>26,27,28,29,30</sup>. We have especially focused on the quantum critical point (QCP) which intervenes the 3-d topological insulator (TI) and an 3-d ordinary insulator. The topological insulator supports a single 2+1 massless surface Dirac fermion for each boundary, while an ordinary insulator does not have any. As such, the bulk wavefunction in those parameter regions (or point) which intervene these two insulating phase should be extended, so as to mediate two opposite surfaces. Such extended bulk states are stable against T-invariant disorders, as far as each surface state in the TI phase is stable. In fact, Nomura et al.<sup>31</sup> and Bardarson et al.<sup>32</sup> have recently calculated the function numerically, and demonstrated that the single-copy of the 2+1 massless Dirac fermion is topologically stable against the T-invariant disorders. This observation strongly indicates that there always exists delocalized (bulk-critical) region between the 3-d

topological insulator phase and an 3-d ordinary insulator phase.

To uncover the nature of this peculiar quantum critical point (or region), we have studied the disorder effect on its minimal model, i.e. the 1-copy of the 3+1 Dirac fermion. As a basis for this, we first studied in the section III how the chemical potential type disorder brings about a finite life time of the zero-energy wavefunction. We then observed that there exists a certain critical disorder strength above which the DOS at the zero-energy becomes finite (see eq. (51)).

When the finite topological mass is introduced, a system eventually enters either the TI or an ordinary insulator, depending on the sign of the topological mass. In Sec. III, we studied how this topological mass are renormalized by the chemical potential-type disorder within the self-consistent Born approximation. By doing this, we have determined the phase boundary between the compressible phase and the gapped phase (see Figs. 9,10).

To further infer the low-energy structure in this compressible phase, we have derived in the section IV the diuson, Cooperon and the weak localization (WL) correction to the electric conductivity. We then observed that the charge diuson mode and parity diuson mode dominant the diuson (see eq. (106)); the charge channel always carries the diuson pole structure, while the parity density channel becomes massless only in the absence of the topological mass. In the presence of the finite topological mass, it generally suffers from the infrared cut-off  $\frac{1}{\text{topo}} / m^2$ .

Corresponding to this feature in the diuson, the Cooperon is also composed of two quasi-degenerate dominant contributions (see eqs. (112-114)). In the zero topo-



logical mass limit, these two contributions bring about the same magnitude of the anti-weak-localization (AWL) correction with each other. When the finite topological mass is introduced, however, that from the parity density channel becomes truncated by the finite infrared cutoff  $\frac{1}{\text{topo}}$ . As such, one half of the AWL correction becomes ineffective. As a result, on increasing  $m$ , the AWL correction exhibits a crossover into one half of its original value ("quantum correction doubling").

### B. "Levitation and pair annihilation" phenomena

Let us discuss open issues in the 3-d  $Z_2$  QSH system in the view point of our findings. As a tightly related topic to the stability of the QCP, the levitation and pair annihilation phenomena of the extended states<sup>33</sup> were recently observed in the 2-d  $Z_2$  quantum spin Hall system by Onoda et al.<sup>26</sup> They numerically studied the disorder effect on the Kane-Mele model<sup>5</sup> on the honeycomb lattice. In the clean case the system is set to be in the QSHI phase; namely, the spectrum consists of two bands, and there is a gap between them. When the system is disordered, some states far from the band centers become localized, while there are energy regions of delocalized states, located at the centers of the upper (empty) band and lower (filled) band. What Onoda et al.<sup>26</sup> have found is that each of these two does not disappear by itself, when the disorder strength is increased. Instead, when the disorder becomes much stronger than the disorder strength for the localization in an ordinary insulator, these two merge into one bundle of extended states energetically, and annihilate in pair (see Fig. 12 (a)).

To argue this phenomena more generally, consider the 3-dimensional parameter space spanned by the topological mass term  $m$ , chemical potential  $\mu$  and disorder strength  $\alpha$ . From the surface-state arguments described in the introduction, two insulating phases having different types of edge (surface) states, i.e. the topological insulator and an ordinary insulator, should be disconnected by the delocalized (bulk-critical) region. Then, when a finite topological mass term  $m$  changes its sign from positive (topological insulator side) to negative (ordinary insulator side), we should also expect that a similar levitation and pair annihilation phenomena occurs. Namely, when a system transits from the topological insulator side to the ordinary insulator side, the region of extended states in the upper band and that in the lower band always merge and annihilate with each other (see Fig. 12 (b)). Combining this picture with the Onoda's numerical observation<sup>34</sup>, one can then expect that the delocalized (bulk-critical) region constitute a surface in the 3-d parameter space spanned by  $\mu$ ,  $m$  and  $\alpha$ , only to isolate the topological insulator phase from an ordinary insulator phase (see Fig. 13).

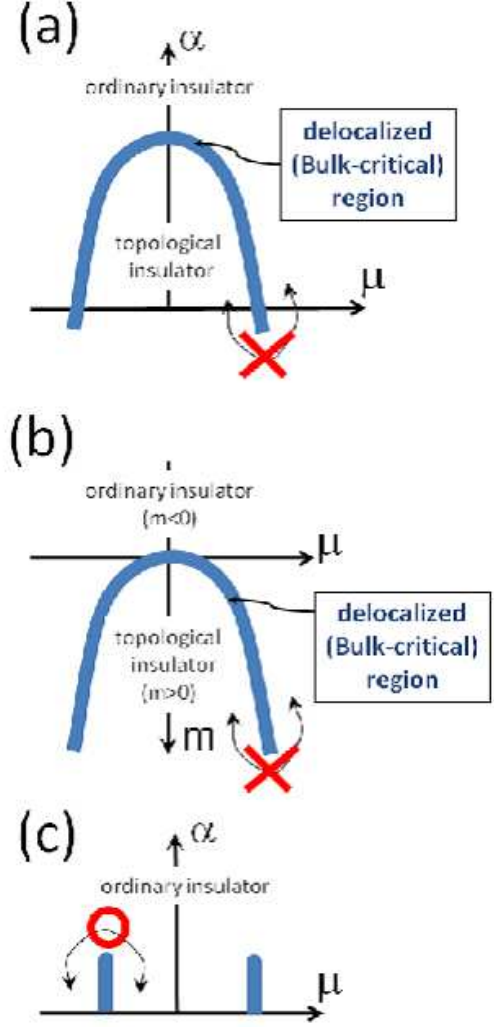


FIG. 12: (a); Onoda's phase diagram<sup>26</sup> in the  $\alpha$ - $\mu$  plane with  $m > 0$  (topological insulator side) (b); A schematic phase diagram in the  $m$ - $\mu$  plane, which is expected from the surface (edge) state's argument described in the section. I. (c); A schematic phase diagram in the  $\alpha$ - $\mu$  plane of the ordinary insulator side ( $m < 0$ ). In (a-c), we have two delocalized energy regions (blue filled regions), which locate at the center of the upper band and the lower band. In (a), these two delocalized regions eventually merge and annihilate in pair, when  $\alpha$  increases. As a result, the topological insulator and ordinary insulator are always disconnected by the bulk-critical (delocalized) region. In (c), however, two delocalized regions registered at the upper band and the lower band annihilate without merging each other, when  $\alpha$  increases. Thus, all the insulating regions appearing in (c) are adiabatically connected from one point to others. In (b), two delocalized regions merge and annihilate with each other, when the topological mass  $m$  changes its sign from positive to negative. As a result, the topological insulator and ordinary insulator are again disconnected from each other by the bulk-critical (delocalized) region, as in (a).

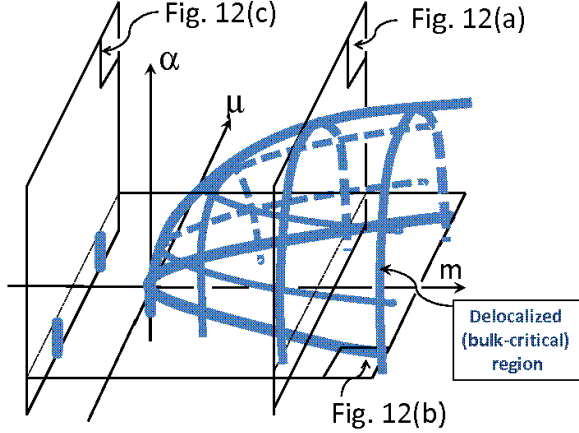


FIG. 13: A Schematic phase diagram in the  $\mu$ - $m$  space. The vertical axis is the disorder strength  $\alpha$ , while the horizontal plane is spanned by the chemical potential  $\mu$  and the topological mass  $m$ . The delocalized region (blue filled region) constitutes a surface in this 3-dimensional parameter space, so that an ordinary insulator phase and the topological insulator phase are adiabatically disconnected from each other. Namely, one cannot move from one phase to the other, without crossing the delocalized region, i.e. bulk-critical region. The phase diagram for the constant positive  $m$  (topological insulator side) and that for the constant negative  $m$  (ordinary insulator side) are separately described in Fig. 12 (a) and (c) respectively. The phase diagram for the constant  $\alpha$  corresponds to Fig. 12 (b).

### C. Possible microscopic scenario

Generally speaking, one has to go beyond our mean-field treatment of disorder in order to study the behaviors of mobility edges. However, we can still speculate the microscopic picture of the "levitation and pair annihilation" phenomena discussed above, in terms of the "quantum correction doubling" found in this paper.

We expect that the intervening bulk-critical region (blue filled region in Figs. 12(a-b) and Fig. 13) corresponds to the  $\frac{1}{\text{topo}} \rightarrow 0$  region. Namely, when a system transits from the topological insulator to an ordinary insulator, we surmise that one of the high-energy modes, i.e. parity diffusion mode appearing in eq. (106), becomes massless once, only to guarantee the existence of the bulk-critical region between these two insulating phases. This conjecture naturally leads to the following microscopic scenario of the "levitation and pair annihilation" phenomena.

Suppose that the  $T$ -symmetric disorder is introduced in the topological insulator. We assume that such disorder potential is strong enough to make the system localized. But it is not strong enough to make the upper (empty) band and low (occupied) band mixed with each other. Namely, a system locates in the topological insulator side of Fig. 12 (a), so that it can be adiabatically connected into the topological insulator phase in the clean

limit. In such localized phase, we expect that a parity diffusion mode always exists in the high energy region and is protected by the infrared cut-off  $\frac{1}{\text{topo}}$ , while the charge diffusion mode disappears because of the relatively strong disorders (see Fig. 14 (a)). Starting from such localized phase, decrease the topological mass term (or further increase the disorder strength). Then, this infrared cut-off  $\frac{1}{\text{topo}}$  associated with the parity diffusion mode decreases gradually, only to be renormalized to be zero at the transition point (see Fig. 14 (b)). Namely, at this transition point, the parity diffusion mode becomes massless. As a result, the Cooperon term corresponding to this parity diffusion mode, i.e. eq. (114), becomes effective and brings about the positive quantum interference effect on the back-scattering processes, in a same way as in the section. IV D. Because of this positive quantum interference effect, which emerges only when the parity diffusion mode becomes massless, the charge diffusion constant recovers at around  $\frac{1}{\text{topo}} \rightarrow 0$ , even in the presence of the relatively strong disorder (see the red line in Fig. 14 (b)).

However, when one further decreases the topological mass (or increases the disorder strength), the infrared cut-off  $\frac{1}{\text{topo}}$  becomes finite again. As a result, this positive quantum interference effect due to the massless parity diffusion mode becomes ineffective again, only to lead a system into an insulating phase (see Fig. 14 (c)). This insulating phase is now adiabatically connected to an ordinary insulator in the clean limit.

To uphold this microscopic picture, we need to consider several ingredients missing in our approach<sup>35</sup>. We will enumerate them in the following. As indicated in Figs. 12-13, the pair-annihilation occurs only in the topological insulator side. Namely, the phase diagram is asymmetric with respect to the sign change of the topological mass term. On the other hand, all the findings in this paper are symmetric with respect to the sign change of this mass term. This is obviously because our starting model is the effective continuum model, describing only the local structure around a certain  $k$ -point. On the other hand, the  $Z_2$  topological number is determined from the global information of the Bloch wavefunctions' phase in the  $k$  space<sup>15</sup>. Therefore, in such an effective continuum model one cannot determine whether the topological insulator by itself corresponds to the  $m > 0$  phase or the  $m < 0$  phase. Instead, it simply dictates that one of these two should be the topological insulator, and the other is an ordinary insulator. As such, to describe the asymmetric behavior of the mobility edge as in Fig. 13, we clearly have to deal with lattice models.

In the present work we treated disorder in the mean-field level, considering only the Cooperon correction. To verify the aforementioned scenario, we thus also need to deal with interactions among the various low-energy modes, beyond the mean-field treatment. In such situations, the inter-mode interaction between the quasi-degenerate Goldstone modes found in the section IV certainly plays an important role in the "levitation and pair annihilation" phenomena.

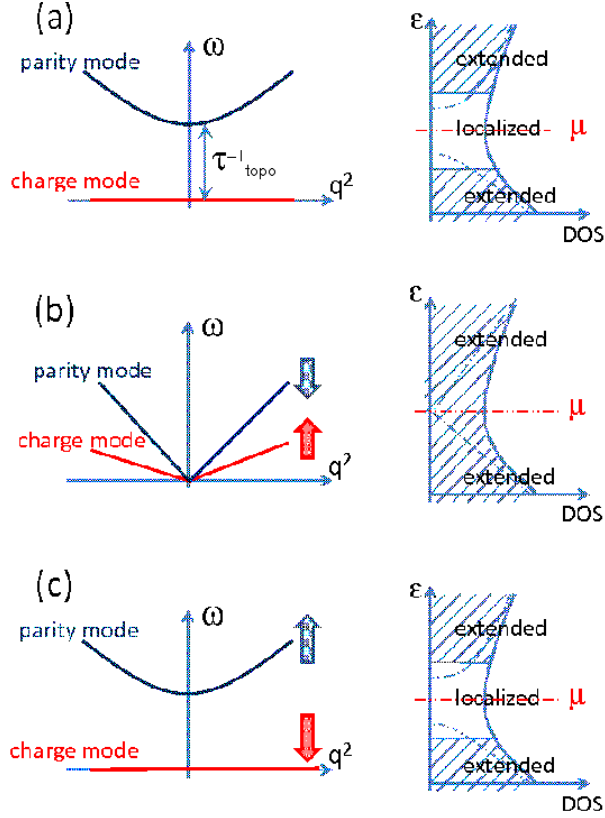


FIG. 14: (a); The low-energy spectrum in the topological insulator side contains two relevant dispersion modes. One is the usual charge dispersion mode, which disappears in the presence of relatively strong disorders. The other is the parity dispersion mode, which is protected by the infrared cut-off  $\tau_{\text{topo}}^{-1}$  from the disorders. (b); When a system transits from the topological insulator phase to the ordinary insulator phase, the parity dispersion mode becomes massless. Namely, when one further increases the disorder, starting from (a),  $\tau_{\text{topo}}^{-1}$  becomes renormalized by the disorder, only to reach zero. As a result, the Cooperon term corresponding to this parity dispersion mode becomes effective and induces the positive quantum interference effect on the backward scattering process of the charge-degrees of freedom. Because of this, the charge dispersion mode recovers at  $\tau_{\text{topo}}^{-1} = 0$ . (c); The low-energy spectrum in the ordinary insulator side.

#### Acknowledgments

We are grateful to Leon Balents, A.P. Schnyder, K-i Imura, Kentaro Nomura, Shinsei Ryu, Hideaki Obose, Akira Furusaki and Hiroshi Kohno for helpful discussions. This research is supported in part by Grant-in-Aids from the Ministry of Education, Culture, Sports, Science and Technology of Japan. RS was financially supported previously by the Osaka University and currently by the Institute of Physical and Chemical Research (RIKEN). Part of this work is done during the ISSP-YITP joint-workshop entitled as "Topological Aspects of Solid State Physics (TA SSP)".

#### APPENDIX A: EFFECTS OF GENERIC TIME-REVERSAL INVARIANT DISORDERS

In this paper, we have restricted ourselves to the chemical potential type disorder for simplicity. However, there exist in general several other types of T-invariant disorder potentials, as described in section II (see eq. (7)). We basically expect that these additional time-reversal invariant disorders will not change our results drastically. To uphold this expectation, we study in this appendix how our self-consistent Born solution is modified in the presence of generic time-reversal invariant disorders, focusing on the zero-energy wavefunction at the critical point. As a result, we will obtain the following facts, which support this expectation. One is that, when only the diagonal correlations,  $\chi_{jj}$ , are present, our solutions derived in section III do not change at all (see eqs. (A16, A4, A8)). When the off-diagonal correlation such as  $\chi_{05}$  is introduced,  $F_5$  acquires a finite imaginary part, i.e.  $F_5^0 \notin 0$ , even at the zero-energy state at the critical point (see eqs. (A16, A4, A8)). However, provided that  $\chi_{05}$  is not so large in comparison with the diagonal correlation such as  $\chi_{00}$ ,  $\chi_{55}$  and etc. the effect of the non-zero  $F_5^0$  is expected to be negligible.

The generic T-reversal invariant disorders bring about the coupling between  $F_5$  and  $F_0$  more explicitly in the self-consistent Born (scB) equation. Namely, instead of eqs. (38-39), our scB equation reads;

$$\sum_{0 < k < 1} d^3k \frac{A + F_0}{F_0^2} \frac{B F_5}{F_5^2} = f_0 - F_0; \quad (\text{A } 1)$$

$$\sum_{0 < k < 1} d^3k \frac{B F_0}{F_0^2} \frac{A F_5}{F_5^2} = f_5 - F_5; \quad (\text{A } 2)$$

where only the following three parameters are the relevant model parameters;

$$A = \chi_{00} + \chi_{55} + \chi_{jj}; \quad (\text{A } 3)$$

$$B = 2\chi_{05}; \quad (\text{A } 4)$$

The coefficients of  $\chi_{1,2,3,4}$  in the 1-point Green function, on the other hand, are again free from renormalization;

$$F_{1,2,3} = \bar{f}_{1,2,3} = k_{1,2,3}; \quad F_4 = \bar{f}_4 = 0; \quad (\text{A } 5)$$

In terms of  $G$  defined in eqs. (40,41), We can rewrite eqs. (A1-A2) more transparently;

$$\begin{pmatrix} 2(A + F_0) & B F_5 \\ 2(B F_0) & A F_5 \end{pmatrix} \begin{pmatrix} G = 0 \\ f_0 \\ f_5 \end{pmatrix} = \begin{pmatrix} F_0 \\ F_5 \end{pmatrix}; \quad (\text{A } 6)$$

When it comes to the zero-energy wavefunction at the critical point, i.e.  $f_0 = f_5 = 0$ , this coupled equation could be "diagonalized";

$$1 - G = F_0 = F_5 = 0; \quad (\text{A } 7)$$

with  $\alpha = \beta$  and  $\gamma$  are defined as follows

$$\frac{1}{B} \left( \frac{P}{s} \frac{B^2}{2} \right); \quad (\text{A } 8)$$

$$\frac{1}{a} \left( \frac{P}{s} \frac{B^2}{2} \right); \quad (\text{A } 9)$$

with positive definite  $s$  and  $a$ ;

$$\begin{aligned} \frac{1}{2} A_+ + A_- &= 00 + 55; \\ \frac{1}{2} A_+ - A_- &= X \end{aligned}$$

$$j2 f15; \quad ;45g$$

Observing eqs. (17), note also that  $s$  defined above is always greater than  $\beta$  defined in eq. (A 4);

$$\frac{2}{s} B^2 > 0; \quad (\text{A } 10)$$

Eq. (A 7) with  $\alpha = \beta$  can be trivially satisfied by  $F_0 = F_5 = 0$ . In what follows, we will enumerate all possible non-trivial solutions of this coupled equation. Let us first write down the real part and imaginary part of Eq. (A 7) for both  $\alpha = \beta$ , separately. Noting that  $\alpha$  and  $\beta$  are real-valued, we have the following for  $\alpha = \beta$ ,

$$\begin{aligned} 1 + \text{Re} G + \text{Im} G + F_0^0 F_5^0 &= 0; \\ + \text{Im} G - 1 + \text{Re} G + F_0^0 F_5^0 &= 0; \end{aligned} \quad (\text{A } 11)$$

For  $\alpha = \beta$ , we have

$$\begin{aligned} 1 + \text{Re} G + \text{Im} G + F_0^0 F_5^0 &= 0; \\ \text{Im} G - 1 + \text{Re} G + F_0^0 F_5^0 &= 0; \end{aligned} \quad (\text{A } 12)$$

Observing eq. (A 10), notice that  $\alpha \neq \beta$  in general. As such,  $(F_0; F_5)$  cannot satisfy  $F_5 = F_0$  and  $F_5 = -F_0$  simultaneously. Thus, when  $F_5 = F_0$  is adopted, the determinant of the  $2 \times 2$  matrix in eq. (A 11) should be zero;

$$\begin{aligned} 1 + \text{Re} G + \text{Im} G &= 0; \\ + \text{Im} G - 1 + \text{Re} G &= 0; \end{aligned} \quad (\text{A } 13)$$

or equivalently

$$1 = -\text{Re} G; \quad \text{Im} G = 0;$$

On the other hand, when  $F_5 = -F_0$  holds true, we have the following in turn,

$$1 = \text{Re} G; \quad \text{Im} G = 0;$$

We thus have the only two possible non-trivial solutions;

- (Bi) :  $F_5 = F_0; 1 = -\text{Re} G$  and  $\text{Im} G = 0$ ;
- (Bii) :  $F_5 = -F_0; 1 = \text{Re} G$  and  $\text{Im} G = 0$ ;

In either cases,  $\text{Im} G = 0$  readily leads us to  $a = 0$  first. The reasoning of this was already described in section IIIA 1. When  $a = 0$ , the real part of the function  $G$

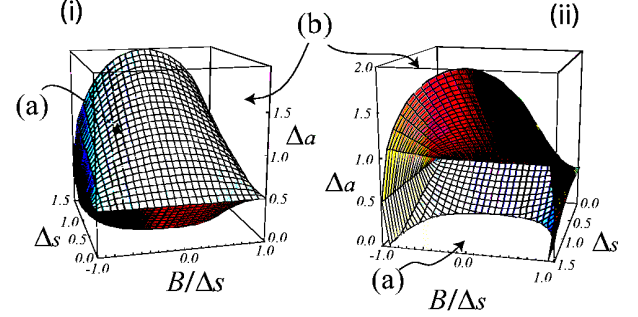


FIG. 15: The phase diagram of the scB solution in the presence of generic time-reversal invariant disorders. The region-(a) includes the "compressible phase" argued in the section III and IV, i.e.  $\alpha > \beta$  and  $B = 0$  and  $a = 0$ . The region-(b) appears only when  $\alpha = \beta$  and  $j2 f15; ;45g jj > 0.5$ . Note also that  $\alpha; s > 0$  and  $B < s$  because of eq. (17) (see also eq. (A 10)).

becomes simplified;  $\text{Re} G_{\alpha=\beta} = 2 + 2bA \text{rcTan} b^{-1}$  (see eq. (43)). Thus, above two solutions will be transcribed into the following two;

$$bA \text{rcTan} [b^{-1}] = \frac{1 + 2}{2}; \quad (\text{A } 14)$$

with  $F_5 = F_0$  respectively.

Since the left hand side of eq. (A 14) is positive semidefinite, we have the following two parameter region supporting non-trivial solutions;

$$\begin{aligned} (a) : \alpha &< \frac{1}{2} < \beta; \\ (b) : \alpha &< \beta < \frac{1}{2}; \end{aligned}$$

We also used  $\alpha > \beta$ , which is trivially supported by eq. (A 10). These two parameter regions are depicted in Fig. 15, where the region-(a) actually includes the "compressible phase" argued in the sections III and IV, i.e.  $\alpha > \beta$  and  $B = a = 0$ .

In this region-(a), only the type-(Bi) solution becomes possible;

$$F_5 = F_0; (a;b) : 0; \frac{1 + 2}{4 +} : \quad (\text{A } 15)$$

Under  $F_0^2 F_5^2 (a + ib)^2$ , this is identical to the following solution;

$$(F_0; F_5) = \frac{bj}{1 - \frac{1}{2}} (1; -) : \quad (\text{A } 16)$$

This solution comprises continuously with the physical scB solution described in the section III. Namely, when  $a$  taken to be zero, eq. (A 16) precisely reduces to eq. (51).

When it comes to the region-(b), type-(Bii) also becomes a possible solution;

$$F_5 = +F_0; (a;b) \rightarrow 0; \frac{+2}{4}; \quad (\text{A } 17)$$

namely,

$$(F_0; F_5) = \frac{+2}{+2+1} ( +^1; 1); \quad (\text{A } 18)$$

In the absence of finite  $B$  and  $a$ , however, this solution is continued into eq. (49). Thus, this can never hold true therein. Because of this, we judge the type-(Bii) solution to be unphysical.

#### APPENDIX B: MODE-MODE COUPLING THEORY

The weak-localization calculation (and also the self-consistent Born calculation) described in the section. IV

has the small coupling constant  $1=(\quad)$  only for the weakly disordered region, i.e.  $< \quad_c$ , while it becomes an uncontrolled analysis for  $> \quad_c$ . Bearing in mind this strong disorder region, we will employ in this appendix more phenomenological calculations, based on the mode-mode coupling theory<sup>23</sup>. Without resorting to the Kubo formula, this theoretical framework gives us a mean-field equation for the diffusion constant  $D$ , where the quantum correction due to the Cooperon term are taken into account as in the standard weak-localization calculation<sup>23</sup>. The final results of this appendix. B such as eqs. (B 54, B 61) indicate that this quantum correction becomes doubled, when the topological mass term are tuned to be zero.

The calculation consists of two steps. The first step begins with the Bethe-Salpeter (BS) equation for the response function  $\chi(k; k^0; q; !);$

$$\chi(k; k^0; q; !) = G^R_{-1}(k_+; +) G^A_{-1}(k; -) \frac{1}{2-i} \frac{1}{1-k; k^0} + \sum_{k_1} U^{2P, IR}_{-1; -1; -1}(k; k_1; q; !) \chi(k_1; k^0; q; !); \quad (\text{B } 1)$$

$$\chi(k; k^0; q; !) = \frac{1}{2-i} G^R(k_+; k^0; +) G^A(k^0; k; -) \chi_{imp}; \quad (\text{B } 2)$$

with  $k = k - \frac{q}{2}$  and  $\frac{1}{2}$ . Out of this equation, we first derive the linearized equations of motion (EOM's) for the density relaxation function  $\chi_0(q; !)$ , current relaxation function  $\chi_j(q; !)$  and relaxation functions associated with other internal degrees of freedom;

$$\chi_0(q; !) = \sum_{k, k^0} \chi^{\wedge_0}(k; k^0; q; !); \quad (\text{B } 3)$$

$$\chi_j(q; !) = \sum_{k, k^0} \hat{q}^j \chi^{\wedge_j}(k; k^0; q; !); \quad (\text{B } 4)$$

with  $\hat{q}$  normalized to be a unit vector. Since the EOM's thus derived are linearized, one can solve them for these relaxation functions, only to obtain their asymptotic expressions for the small  $q, !$ ;

$$\chi_0(q; !) = \frac{1}{! + iD q^2}; \quad \chi_j(q; !) = \frac{q_j}{! + iD q^2};$$

To be more specific, the diffusion constant  $D$  appearing in the denominators will be expressed in terms of the relaxation kernels  $M_{ab}(q; !)$ , latter of which are defined by the two-particle irreducible (2P IR) vertex function  $\hat{U}^{2P, IR}$

(step-(i));

$$D = \frac{1}{M_{jj} M_{5j; 5j} M_{5j; j} M_{jj; 5j}} \frac{M_{5j; 5j}}{M_{5j; j} M_{jj; 5j}} \chi_{jj; 0}; \quad (\text{B } 6)$$

$$M_{ab}(q; !) = 2i \frac{1}{ab} + \frac{1}{2^4} \sum_{k, k^0} \frac{L_a(k; q; !)}{U^{2P, IR}_j(k; k^0; q; !)} R_b(k^0; q; !); \quad (\text{B } 7)$$

(see also eqs. (B 31-B 32) for the definitions of  $\hat{L}_a^{L, R}$ ).

The 2P IR vertex function  $\hat{U}^{2P, IR}(k; k^0; q; !)$  in disordered media is usually dominated by the Cooperon at small  $!$  and  $k + k^0$ . The Cooperon is the series-sum of the ladder-type diagrams in the particle-particle channel, which is therefore obtained from the diffusion with the hole-line time-reversed. The diffusion is in turn responsible for the diffusion pole in the relaxation functions, i.e. the denominators in eq. (B 5). As such, in the presence of the T-symmetry, the asymptotic form of the Cooperon at small  $!$  and  $k + k^0$  should be characterized by the same diffusion constant as that in eq. (B 5). Based on this spirit, we will replace the 2P IR vertex function in eq. (B 7) by this asymptotic form of the Cooperon. Through this

approximation, eqs. (B 6-B 7) constitute a self-consistent equation for the diffusion constant  $D$  (step-(ii)).

As we have seen explicitly in section. IV, the diffusion consists of the charge diffusion mode and parity diffusion mode;

$$\hat{G}^d(q;!) / \frac{1}{1 + iD q^2} \hat{G}_1^d + \frac{1}{1 + iD q^2 + i \frac{1}{\tau_{\text{topo}}}} \hat{G}_2^d; \quad (\text{B } 8)$$

with the positive semidefinite  $\frac{1}{\tau_{\text{topo}}}$  proportional to  $m^2$  (see eqs. (104,107-108)). Namely, the second term, i.e. the parity diffusion mode, generally suffers from the finite infrared cut-off in the presence of the topological mass. While both of these two equally dominates the low-energy region for  $m \rightarrow 0$ ;

$$\hat{G}^d(q;!) / \begin{cases} \frac{1}{1 + iD q^2} \hat{G}_1^d + \hat{G}_2^d & \text{for } D \ll \frac{1}{\tau_{\text{topo}}}; \\ \frac{1}{1 + iD q^2} \hat{G}_1^d & \text{for } D \gg \frac{1}{\tau_{\text{topo}}}; \end{cases} \quad (\text{B } 9)$$

(see eqs. (102,98) and eq. (106)). In the presence of the  $T$ -symmetry, this crossover behaviour will be transcribed onto the Cooperon term; the backward scattering process originated from the parity diffusion mode becomes ineffective, in the presence of the relatively large topological mass;

$$\hat{U}^{\text{coop}}(k + k^0;!) / \begin{cases} \frac{1}{1 + iD (k + k^0)^2} \hat{U}_1^c + \hat{U}_2^c & \text{for } D \ll \frac{1}{\tau_{\text{topo}}}; \\ \frac{1}{1 + iD (k + k^0)^2} \hat{U}_1^c & \text{for } D \gg \frac{1}{\tau_{\text{topo}}}; \end{cases}$$

(see eq. (112)).

Corresponding to these two-mode features, we will derive in this appendix the two limiting gap equations; one is valid for  $D \ll \frac{1}{\tau_{\text{topo}}}$ , while the other is for  $D \gg \frac{1}{\tau_{\text{topo}}}$ . This appendix is organized as follows. The appendix. B1 is devoted for the step-(i), in which the linearized coupled EOM's for the relaxation functions and eqs. (B 6-B 7) will be derived. Using eqs (B 6-B 7), we will derive in the appendix. B2 the gap equations for the two-limiting cases (step-(ii)). By solving these gap equations, we will finally see how the diffusion constant for  $\gamma > \gamma_c$  behaves as a function of  $\gamma$  and  $m$  (see eqs. (B 54, B 61) and Fig.18).

### 1. Coupled EOM's for relaxation functions

The EOM's derived henceforth are linearized with respect to the relaxation functions (unknown quantities). Namely, the mode-mode interactions among various bosonic degrees of freedom (density, current and so on) will be represented by the mean-field induced by the corresponding relaxation functions. This mean-field for the relaxation function is analogous to the self-energy for a 1-point Green function, so that it is often dubbed as the relaxation kernel<sup>23</sup>. Being linearized, such EOM's can be

easily solved, only to let us express relaxation functions in terms of the relaxation kernel.

These linearized EOM's also have to be closed with respect to a set of unknown relaxation functions. Consider, for example, the EOM of the density relaxation function, which is nothing but the continuity equation. This equation contains the current relaxation function. Accordingly, to make coupled EOM's to be closed, we further need the EOM for this current relaxation function, i.e. constitutive equation. The constitutive equation usually involves interactions between the current and other degrees of freedom (DOF's) such as the spin density, sublattice density and so forth. As such, we further need to derive the EOM's of the relaxation functions associated with these internal DOF's. In this way, we need to make our entire coupled EOM's to be closed with respect to a set of unknown relaxation functions.

Let us begin with the continuity equation. Apply the following differential operator from the left hand side of the Bethe-Salpeter equation eq. (B 1);

$$\begin{aligned} \hat{G}_0^{-1}(k; q;!) &= \hat{G}^R(k; +) \hat{G}^A(k; -) \\ &= \hat{1} \hat{q} \hat{G}^R(+) + \hat{G}^A(-): \end{aligned}$$

Taking the summation over repeated band indices, we then have;

$$\begin{aligned} &\hat{1} \hat{q} \hat{G}^R(+) + \hat{G}^A(-); \quad (k; k^0; q;!) \\ &= \hat{G}^R(k; +) \hat{G}^A(k; -) \sum_{k^0} \frac{1}{2i} \frac{1}{i} k^0 \\ &+ \sum_{k_1} U_{11;11}^{2P,IR}(k; k_1; q;!) \sum_{k_1} \hat{G}^R(k_1; k^0; q;!) \quad (\text{B } 10) \end{aligned}$$

Under the integrals over  $k$  and  $k^0$ , the vertex function and the self-energy in eq. (B 10) set each other;

$$\begin{aligned} &\hat{1} \hat{q} \hat{G}^R(+) \hat{G}^A(-) \\ &= \frac{1}{2i} \sum_{k^0} \hat{G}^R(k^0; +) \hat{G}^A(k^0; -); \quad (\text{B } 11) \end{aligned}$$

Namely, we used the following Ward identity;

$$\begin{aligned} &\hat{G}^R(k; +) \hat{G}^A(k; -) \\ &= \sum_{k^0} \hat{G}^R(k^0; q;!) U_{00}^{2P,IR}(k^0; k; q;!); \end{aligned}$$

with  $\hat{G}(k; q;!) = \hat{G}^R(k; +) \hat{G}^A(k; -)$ .

Recall that we are interested in the relaxation functions for sufficiently low-energy and long wave-length region; only to derive their diffusion pole structure. Thus, regarding  $\hat{1}$  and  $\hat{q}$  as sufficiently small quantities, we can replace the right hand side of eq. (B 11) by the spectral function;

$$\hat{1} \hat{q} \hat{G}^R(+) \hat{G}^A(-) = A_0 + O(q;!); \quad (\text{B } 12)$$

where  $A_0$  stands for the density of state at  $\epsilon = 0$ ;

$$A_0 = \frac{1}{2i} \sum_k \text{Tr} \hat{G}(k; 0; 0) = 16F_0^{\text{00}}; \quad (\text{B } 13)$$



Eq. (B 12) is nothing but the continuity equation.

The continuity equation derived above contains the current relaxation function. Thus, we need to next derive an equation of motion for this. The derivation goes along in a quite analogous way as that of the continuity equation. Specifically, to end up with an equation having  $\hat{G}^{-1}(k; q; !)$ , we will apply the following onto the Bethe-Salpeter equation, instead of  $\hat{G}^{-1}$ ;

$$\hat{G}^{-1}(k; q; !) = \frac{1}{2} \hat{G}^{-1}(k; q; !); \hat{q}^{\wedge} + :$$

Since  $!$  and  $q$  being sufficiently small, we will keep only its leading-order contributions;

$$\hat{G}^{-1}(k; q; !)' = \left( \frac{\partial F_0^0}{\partial} + 2iF_0^{\infty} \right) \hat{q}^{\wedge} \hat{q}^{\wedge} : \quad (B 14)$$

Apply this onto eq. (B 1) and take the sum over  $k, k^0$  and the band indices. By way of this, we obtain the following constitutive equation;

$$\begin{aligned} & \left( \frac{\partial F_0^0}{\partial} + 2iF_0^{\infty} \right) \hat{G}^{-1}(q; !)' = \hat{q}^{\wedge} \hat{q}^{\wedge} : \\ & = A_j \sum_{k, k_1} \hat{G}_j^L(k; q; !)'_{1,1} \\ & U_{1,1;1,1}^{2P,IR}(k; k_1; q; !)'_{1,1} ;_{1,1}(k_1; k^0; q; !)'_{1,1} \end{aligned} \quad (B 15)$$

$A_j$  and  $\hat{G}_j^L(k; q; !)$  are defined as follows;

$$\begin{aligned} A_j &= \frac{1}{2} \sum_k \text{Tr} \hat{G}_j^L(k; q; !)' ; \quad (B 16) \\ \hat{G}_j^L(k; q; !)' &= \frac{1}{2} \\ \hat{G}(k; q; !)' &= \hat{G}^R(k_+; +) \hat{q}^{\wedge} \hat{G}^R(k_+; +) + \\ \hat{G}^A(k; -) \hat{q}^{\wedge} \hat{G}^A(k; -) &= \hat{G}(k; q; !)' \end{aligned} \quad (B 17)$$

Contrary to the continuity equation, this equation of motion contains the convolution between the 2PIR vertex function and the response function explicitly. This convolution part describes the interactions between the current relaxation function and the other types of relaxation functions. We will linearize this convolution part with respect to relaxation functions in the following three paragraphs.

To do this, note first the completeness of the matrices,

$$\delta_{0,0} = \frac{1}{4} \sum_{l,m} \hat{Y}_{lm}(\hat{k}) \hat{Y}_{lm}(\hat{k}^0) = \delta_{0,1}; \delta_{5,15}; \delta_{4,2} \quad (B 18)$$

and that of the spherical harmonic function  $Y_{lm}(\hat{k})$ ,

$$f(\hat{x}) = \sum_{l=0}^{\infty} \sum_{m=-l}^l Y_{lm}(\hat{x}) \sum_{l=0}^{\infty} Y_{lm}(\hat{x}^0) f(\hat{x}^0); \quad (B 19)$$

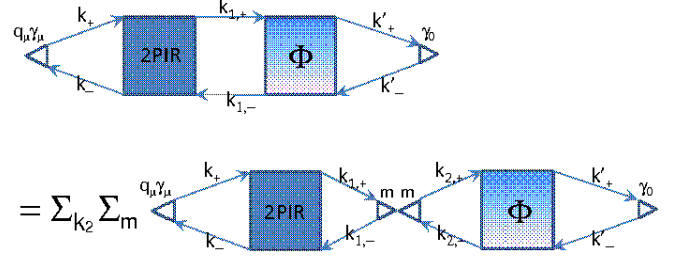


FIG. 16: The convolution between the 2PIR vertex function and the response function is replaced by the direct product between the relaxation kernels and relaxation functions, where we used the complete set for a function of  $k_1$ , i.e.  $f(k_1) = \sum_{k_2} (k_1 - k_2) f(k_2) = \sum_{k_2, m} u_m(k_1) u_m(k_2) f(k_2)$ . Namely,  $u_m$  constitutes the bare vertex part described by  $\backslash$ -mark in the figure, while  $u_m$  constitutes that described by  $/$ -mark

where  $\hat{k}$  denotes the normalized vector and  $\int \hat{k}^{\wedge}$  stands for the 2-dimensional integral over the angle-direction;  $\int \hat{k}^{\wedge} = 4$ . Using these two completeness relations, we can decouple the convolution part in eq. (B 15) into the sum over the countable numbers of modes (see also Fig. 16);

$$\begin{aligned} & \left( \frac{\partial F_0^0}{\partial} + 2iF_0^{\infty} \right) \hat{G}^{-1}(q; !)' = \hat{q}^{\wedge} \hat{q}^{\wedge} : \\ & = A_j \sum_{k, k_1} \hat{G}_j^L(k; q; !)'_{1,1} U_{1,1;1,1}^{2P,IR}(k; k_1; q; !)'_{1,1} \\ & = \sum_{l=0}^{\infty} \sum_{m=-l}^l Y_{lm}(\hat{k}_1) \hat{Y}_{lm}(\hat{k}) \sum_{l=0}^{\infty} \sum_{m=-l}^l Y_{lm}(\hat{k}^0) f(\hat{x}; q; !)'_{1,1} : \end{aligned} \quad (B 20)$$

Namely, the  $k_1$ -dependence of the response function is decomposed into the dependence on its radial coordinate  $|\hat{k}_1|$  and that on the angle coordinate  $\hat{k}_1$ . At a price for this, the right hand side contains the summation over the azimuthal and magnetic quantum numbers,  $l$  and  $m$ . For each  $l, m$  and  $\hat{k}_1$ ,  $\hat{Y}_{lm}(\hat{x}; q; !)'_{1,1}$  is defined as follows;

$$\hat{Y}_{lm}(\hat{x}; q; !)'_{1,1} = \sum_{k^0} \hat{Y}_{lm}(\hat{k}) f(\hat{x}; q; !)'_{1,1}; \quad (B 21)$$

Observing this definition, notice that the  $x$ -dependence of  $\hat{Y}_{lm}(\hat{x}; q; !)'_{1,1}$  and its  $!$ ,  $q$ -dependence can be further factorized for small  $!$  and  $q$ ;

$$\hat{Y}_{lm}(\hat{x}; q; !)'_{1,1} = g_{lm}(\hat{x}) \hat{Y}_{lm}(\hat{k}); \quad (B 22)$$

This is because, for such small  $!$  and  $q$ , the response function appearing in eq. (B 21) is dominated by the disson,

which depends only on  $l$  and  $q$ ;

$$; (k; k^0; q; l) = \frac{1}{2} \frac{\hat{G}^R_{l-1}(k_+; +) \hat{G}^A_{l-1}(k_-; -)}{\hat{G}^R_{l-1}(k_+^0; +) \hat{G}^A_{l-1}(k_-^0; -)}; \quad (B23)$$

By taking the integrals over  $\hat{k}$  and  $k^0$  in eq. (B21) and keeping only the leading order in small  $l$  and  $q$ , one can actually verify this factorization for any  $l, m$  and (consult also the appendix D for several examples.)

Without loss of generality, we can assume that  $g_{lm}; (x)$  thus obtained is normalized with respect to the integral over the radial direction;

$$\int_0^\infty x^2 dx g_{lm}; (x) = 1;$$

Then, corresponding  $g_{lm}; (q; l)$  given in eq. (B22) becomes the non-zero azimuthal number ( $l \neq 0$ ) generalizations of the relaxation functions defined in eqs. (B3, B4);

$$g_{lm}; (q; l) = \sum_{k; k^0} \hat{Y}_{lm}(\hat{k}) ; (k; k^0; q; l); \quad (B24)$$

Thus, substitute eq. (B22) back into eq. (B20). Then, we finally obtain the constitutive equation, which is fully linearized with respect to these relaxation functions;

$$\left( i \frac{\partial F_0^0}{\partial t} + 2iF_0^0 \right) j(q; l) - q_0(q; l) = A_j \frac{1}{4} \sum_{l=0}^\infty \sum_{m=-l}^l \sum_{k; k^0} \hat{Y}_{lm}(\hat{k}) U_{j; }^{2P, IR} (k; k^0; q; l) + \sum_{l=0}^\infty \sum_{m=-l}^l g_{lm}; (k^0) Y_{lm}(\hat{k}^0) g_{lm}; (q; l); \quad (B25)$$

The second member of its right hand side described the 'mean-field' induced by other relaxation functions, into which the 2P-IR vertex function is encoded. This situation is quite analogous to how the 1-particle irreducible function (i.e. self-energy) describes the interaction among 1-point Green functions.

Due to this interaction, however, the constitutive equation above also contains relaxation functions  $g_{lm}; (q; l)$  assigned to the higher order harmonic ( $l \geq 1$ ) sector. Thus, to make the final coupled EOM's to be closed, we must also derive the EOM for all of these functions. This is, however, limitless. To make it tractable, we thus need to truncate interactions among these too many modes. In this paper, we will consider the interactions only within the 's-wave' sector. Namely, we will restrict the summation over  $l, m$  and  $l$  in eq. (B25) to the  $l=0$  sector;

$$; (q; l) = \sum_{k; k^0} \hat{Y}_{00}(\hat{k}) ; (k; k^0; q; l);$$

These 16 modes in the s-wave sector further reduce into the 8 modes, when the rotational symmetry is taken into account. Namely, by noting that the response function is

invariant under the simultaneous rotation in the pseudo-spin space and in the momentum space;

$$\hat{U}_{n; }^x \hat{U}_{n; }^y ; (k; k^0; q; l) \hat{U}_{n; }^y \hat{U}_{n; }^x ; (k; k^0; q; l); \quad (B26)$$

we can derive the following identity;

$$\sum_{a=0}^5 \hat{X}_a^{15} (q; l) = \frac{1}{4} \sum_{a=0}^5 \hat{X}_a^5 (q) \hat{X}_a^5 (q; l); \quad (B27)$$

with:

$$\hat{X}_a^5 (q; l) = \sum_{k; k^0} \hat{X}_a^5 (q) ; (k; k^0; q; l);$$

$$(\hat{X}_0; \hat{X}_5; \hat{X}_4; \hat{X}_{45}) = (\hat{X}_0; \hat{X}_5; \hat{X}_4; \hat{X}_{45})$$

$$(\hat{X}_j; \hat{X}_{5j}; \hat{X}_{4j}; \hat{X}_{45j}) = \hat{X}_j^5 ; \hat{X}_5^5 ; \hat{X}_4^5 ; \frac{1}{2} \hat{X}_{45}^5 ;$$

By use of this equality, eq. (B25) turns out to consist

label	density	T	I	label	\current"	T	I
\0"	$\hat{X}_0$	+	+	\j"	$\hat{X}_j^5$		
\5"	$\hat{X}_5$	+	+	\5j"	$\hat{X}_5^5$	+	
\4"	$\hat{X}_4$			\4j"	$\hat{X}_4^5$		+
\45"	$\hat{X}_{45}$	+		\45j"	$\hat{X}_{45}^5$		+

TABLE III: Symmetry of eight modes in the s-wave sector and their symmetries under the spatial inversion  $I$  and the time-reversal  $T$ . Since  $\hat{X}_0, \hat{X}_4, \hat{X}_5$  and  $\hat{X}_{45}$  behave as a scalar quantity under the rotation defined in eq. (23), we regard them as the '\density' associated with the sublattice and spin degrees of freedom. Corresponding to these four types of density, we have 4 types of '\current"', which in turn behave as a vector quantity under the rotation.

only of those 8 functions defined in eq. (B28);

$$i \frac{\partial F_0^0}{\partial t} j(q; l) - q_0 + \sum_{a=0;5;4;45} M_{j;a} (q; l) \hat{X}_a^5 = A_j; \quad (B29)$$

$$M_{a;b} (q; l) = 2iF_0^0 ab + \frac{1}{2^4} \sum_{k; k^0} \hat{Y}_a^L (k; q; l) U_{j; }^{2P, IR} (k; k^0; q; l) \hat{Y}_b^R (k^0; q; l); \quad (B30)$$

$\hat{Y}_a^L (k; q; l)$  above are given as follows;

$$\hat{Y}_a^L (k; q; l) = \frac{1}{2} \hat{G}^R (k; q; l) \hat{G}^R (k_+; +) \hat{Y}_a(q) \hat{G}^R (k_+; +) + \hat{G}^A (k; -) \hat{Y}_a(q) \hat{G}^A (k_-; -) \hat{G}^R (k; q; l); \quad (B31)$$

$$\hat{Y}_a^R (k; q; l) = \hat{Y}_a(q) g_{00;a} (k); \quad (B32)$$



$M_{a,b}(q;!)$  defined in eq. (B 30) generally appears in the EOM for the  $v_a$ -type relaxation function and plays role of the 'mean-field' induced by the  $v_b$ -type relaxation functions. Namely, this  $8 \times 8$  matrix is nothing but the 'self-energy' in the matrix-form ed EOM 's for the s-wave sector (see eq. (B 35)). Thus, we will refer to  $\hat{M}(q;!)$  as the relaxation kernel henceforth. Before deriving the remaining 6 constitutive equations, let us remark on the general property of this kernel. Observing eq. (B 30), notice that each element of this matrix becomes pure imaginary, when its two arguments taken to be zero;

$$M_{a,b}(q;!) = M_{a,b}(q;!)^* \quad (\text{B 33})$$

This can be directly seen from ;

$$\hat{G}(k;q;!)^T = \hat{G}(k;q;!)^T : \quad U^{2P,IR}_i(k;k^0;q;!) = U^{2P,IR}_i(k;k^0;q;!)^* \quad (\text{B 34})$$

The EOM 's for the other 6 s-wave modes can be derived in parallel with that for the current relaxation function. Specially, we will begin with the Bethe-Salpeter equation applied by the following, instead of eq. (B 14);

$$a\hat{G}^{-1}(k;q;!) = \frac{1}{2} \hat{G}^{-1}(k;q;!) + \hat{v}_a(q) + ;$$

with  $\hat{v}_a(q)$  taken to be  $\hat{v}_5; \hat{v}_4; \frac{1}{2}\hat{q}; \hat{v}_a(q) +$  respectively. Going through the same procedure as described so far, we will reach the constitutive equations for these remaining 6 modes. Combined with eq. (B 12) and eq. (B 29), such equations consist of the following 8 by 8 matrix-form ed EOM 's;

$$\hat{K}(q;!) + \hat{M}(q;!) \hat{A}(q;!) = \hat{A}(q;!) \quad (\text{B 35})$$

$\hat{A}(q;!)$  and  $\hat{A}(q;!)$  have the eight components;

$$\hat{A}^T = \begin{pmatrix} 0; j; 5; 5j; 4; 4j; 45; 45j \end{pmatrix}; \quad \hat{A}^T = \begin{pmatrix} A_0; A_j; A_5; A_{5j}; A_4; A_{4j}; A_{45}; A_{45j} \end{pmatrix};$$

latter of which is defined as follows;

$$A_a(q;!) = \frac{1}{2} \text{Tr} \hat{A}_a^L(k;q;!) : \quad (\text{B 36})$$

$\hat{K}(q;!)$  and  $\hat{M}(q;!)$  are defined as follows;

$$\hat{K} = \begin{pmatrix} \hat{K}_1 & \hat{0} \\ \hat{0} & \hat{K}_2 \end{pmatrix}; \quad \hat{M} = \begin{pmatrix} \hat{M}_1 & \hat{0} \\ \hat{0} & \hat{M}_2 \end{pmatrix}; \quad (\text{B 37})$$

$$\hat{K}_2 = \begin{pmatrix} 2 & 3 \\ 6 & 6 \\ 6 & 4 \end{pmatrix} \begin{pmatrix} !c^{-1} & !c^{-1} & !d^{-1} + 2ie^{-1} \\ !d^{-1} + 2ie^{-1} & q & !c^{-1} \\ 0 & 0 & 0 \end{pmatrix}; \quad \hat{M}_1 = \begin{pmatrix} 6 & 6 \\ 6 & 4 \end{pmatrix} \begin{pmatrix} M_{j,j} & M_{j,5j} \\ M_{5,j} & M_{5,5j} \end{pmatrix}; \quad (\text{B 38})$$

with

$$c^{-1} = \frac{\partial F_0^0}{\partial}; \quad d^{-1} = \frac{\partial F_5^0}{\partial}; \quad e^{-1} = F_5^0; \quad (\text{B 39})$$

By solving eq. (B 35), one can obtain the asymptotic expressions for the relaxation functions for small  $!$  and  $q$ ;

$$_0(q;!) \sim \frac{A_0}{! + iDq^2}; \quad _5(q;!) \sim \frac{A_0 B_0}{! + iDq^2}; \quad (\text{B 40})$$

where  $A_0$  stands for the density of state (see eq. (B 13)). The (renormalized) diffusion constant  $D$  used above and other coupling constants are expressed only in terms of the relaxation kernels estimated at  $!; q = 0$ ;

$$D = i \frac{M_{5j,5j}}{M_{jj}M_{5j,5j} - M_{5j,j}M_{j,5j}}; \quad j,j! = 0 \quad (\text{B 41})$$

$$B_0 = \frac{2iF_5^0 + M_{5,0}}{M_{5,5}}; \quad q;! = 0 \quad (\text{B 42})$$

Eq. (B 41) and eq. (B 30) become the essential building blocks of our gap equation (see below).

## 2. gap equation and its solution

When the non-crossing approximation is employed for the 1-point Green function, the diffusion pole in eq. (B 40) should be attributed to the ladder-type diagram whose long-wavelength expressions were already obtained in sec. IV. Especially, we have observed that in the section. IV B that the charge diffusion mode and parity diffusion mode equally dominates the diffusion in the massless case ( $D \propto \frac{1}{\text{topo}}$ ), while the parity mode becomes ineffective in the presence of the relatively large topological mass ( $D \propto \frac{1}{\text{topo}}$ ) (see eqs. (106,98,102)). Corresponding to these two limiting cases, we will derive two types of gap equations and their solutions in this section.

### a. $m = 0$ case

Let us begin with the zero topological mass case first. In this case, we will sum up eq. (107) and eq. (108), since

$f_3 = f_4$ . With use of eq. (96) and  $a_{2;3;4} = 0$ , such a summand takes on a following form;

$$\hat{d}(q;!)_{F_5=0} = \frac{a_0 f_4}{4} \hat{1} + \hat{T}_1 + \hat{S}_1 + \hat{S}_2 : \quad (\text{B43})$$

In section. IV B, we have observed that the overall factor,  $a_0 f_4$ , has the diusion pole as in eq. (98), where its bare expression were calculated explicitly. Namely, by keeping track of the small  $q$  effect in eq. (78), we obtained the bare diusion constant as in eq. (99). Instead of such bare expressions, however, we will describe henceforth this  $a_0 f_4$  in terms of the renormalized diusion constant defined by eq. (B41). Namely, we want  $a_0 f_4$  to be given by the relaxation kernels, only to obtain the self-consistent equation for the diusion constant.

To do this, notice that relaxation functions for small  $q$  and  $!$  are dominated by the diusion as in eq. (B23). Thus, by substituting eq. (B43) into eqs. (B23,B3), we will first express the density relaxation function in terms of  $a_0 f_4$ ;

$$\rho(q;!) = 64 i^{-2} a_0 f_4 : \quad (\text{B44})$$

The factor  $i^{-2}$  in the right hand side stems from the momentum integral over  $k$  and  $k^0$  in eq. (B3);  $i$  is the ultraviolet cutoff of the momentum-integral. Then, we will equate this with  $\rho(q;!)$  obtained in the step-(i), i.e. eq. (B40). By doing this,  $a_0 f_4$  is expressed in terms of relaxation kernels;

$$64 i^{-2} a_0 f_4 = \frac{1}{2} \frac{A_0}{! + iD q^2} : \quad (\text{B45})$$

Namely, the diusion constant  $D$  in the right hand side was already given by the relaxation kernels as in eq. (B41).

Substituting this back into eq. (B43), we obtain the asymptotic form of the diusion;

$$\begin{aligned} \hat{d}(q;!) &= \frac{a_0 f_4}{4} \hat{1} + \hat{T}_1 + \hat{S}_1 + \hat{S}_2 \\ &= \frac{1}{2^8} \frac{1}{i^{-2} ! + iD q^2} \hat{1} + \hat{T}_1 + \hat{S}_1 + \hat{S}_2 : \quad (\text{B46}) \end{aligned}$$

When its hole line time-reversed, the corresponding Cooperon at small  $!$  and  $k + k^0$  is also derived;

$$\begin{aligned} \hat{U}^{\text{coop}}(k + k^0;!) &= \frac{a_0 f_4}{4} \hat{1} - \hat{T}_1 - \hat{S}_1 + \hat{S}_2 \\ &= \frac{1}{2^8} \frac{1}{i^{-2} ! + iD (k + k^0)^2} \hat{1} - \hat{T}_1 - \hat{S}_1 + \hat{S}_2 \quad (\text{B47}) \end{aligned}$$

where we used the following identities;

$$\begin{aligned} \hat{1} &\hat{S}_0 \hat{T}_1; ; \quad \hat{1} \hat{S}_0 \hat{T}_1; ; 00; \\ \hat{1} &\hat{S}_0 \hat{S}_1; ; \quad \hat{1} \hat{S}_0 \hat{S}_1; ; 00; \\ \hat{1} &\hat{S}_0 \hat{S}_2; ; \quad \hat{1} \hat{S}_0 \hat{S}_2; ; 00; \end{aligned}$$

The diusion constant  $D$  in eq. (B47) is now given by the relaxation kernels, via eq. (B41). These relaxation kernels are in turn defined by the 2PIR vertex function, via eq. (B30). The 2PIR vertex function is usually dominated by the Cooperon given by eq. (B47), at around  $k + k^0 \rightarrow 0$ . As such, we will replace (approximate) the 2PIR vertex function in eq. (B30) by this asymptotic form of the Cooperon, i.e. eq. (B47). By way of this, we obtain closed coupled equations for the (renormalized) diusion constant  $D$ ;

$$D = \frac{i}{M_{jj} M_{5j;5j}} \frac{M_{5j;5j}}{M_{5j;5j} M_{Zj;5j}} ; \quad (\text{B48})$$

$$\begin{aligned} M_{a;b} &= 2iF_0^{00} a;b + \frac{A_0 j}{2^{12} 2^2 D^2} \int_{L^{-1} < k+k^0 < L^{-1}} d^3 k d^3 k^0 \\ &\frac{\hat{A}_a^L(k) \hat{1} - \hat{T}_1 - \hat{S}_1 + \hat{S}_2}{k + k^0^2} ; \quad \frac{\hat{A}_b^R(k^0)}{k + k^0^2} : \quad (\text{B49}) \end{aligned}$$

Since eq. (B47) is valid only for small  $k + k^0$ , we have imposed the additional constraint  $k + k^0 < L^{-1}$  into these integral variables. One might regard this upper limit as the mean-free path. We have already taken in eq. (B49) both  $!$  and  $q$  to be zero. Thus,  $\hat{A}_b^R(k)$  in the right hand side stands for  $\hat{A}_b^R(k;q;!)$  estimated there;

$$\begin{aligned} \hat{A}_a^L(k) &= \hat{A}_a^L(k;0;0); \\ \hat{A}_a^R(k) &= \hat{A}_a^R(k;0;0); \end{aligned}$$

where  $\hat{A}_a$  was already defined in eq. (B28). The normalized real-valued function  $g_{00;a}(x)$  used above is given only in terms of  $F_0$ . For example,  $g_{00;j}(x)$  is given as follows,

$$g_{00;j}(x) = \frac{4}{N_j} \frac{1}{F_0^2} \frac{1}{x^2 j^2} \left( 1 + \frac{8}{3} \frac{x^2 F_0^{02}}{F_0^2 x^2 j^2} \right)^0 ; \quad (\text{B50})$$

with its normalization factor  $N_j$ ;

$$N_j = \frac{1}{F_0^{00}} \left( 1 + \frac{1}{3} \frac{F_0^{02}}{F_0^{00}} \right)^0 : \quad (\text{B51})$$

(see the appendix. D for its derivation). Thus, eqs. (B48–B49) constitute closed coupled equations for the diusion constant.

To solve this gap equation, notice first that the coupling between the current and the  $\hat{S}$ -type current is disconnected in the massless case;  $M_{j;5j} = 0$ . This can be seen directly from

$$\hat{1} - \hat{T}_1 - \hat{S}_1 + \hat{S}_2 ; \quad \hat{q} \cdot \hat{S} = 0 : \quad (\text{B52})$$

which leads to  $D = iM_{jj}$ . As a result of this, eqs. (B48–B49) becomes linear in  $D$ ;

$$\begin{aligned} \frac{1}{D} &= 2F_0^{00} \frac{A_0 F_0^{00}}{2^7 2^2 D^2} \frac{1}{2} \int_{L^{-1} < k+k^0 < L^{-1}} d^3 k d^3 k^0 \\ &\frac{g_{00;j}(k^0)}{k + k^0^2} \left( \frac{(F_0^{00})^2}{(F_0^{00})^2} \frac{(F_0^{00})^2 + k^2}{k^2} + \frac{2(k \cdot \hat{q})}{4(F_0^{00})^2 (F_0^{00})^2} \right) \quad (\text{B53}) \end{aligned}$$

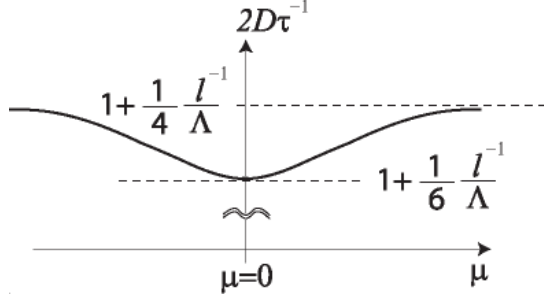


FIG. 17: A schematic plot of  $2D\tau^{-1}$  as a function of the chemical potential in the massless case.

Using eqs. (B 50-B 51), we can readily evaluate the momentum integral in the right hand side of eq. (B 53). To do this, introduce a new integral variable  $q^0 = k + k^0$ , so that  $dk dk^0 = dk dq^0$ . Moreover, we approximate  $g_{00;j}(k - q^0)$  in the integrand by  $g_{00;j}(k)$ , since  $g_{00;j}(x)$  is a slowly varying function in the scale of  $l^{-1}$ . These treatments give us the following expression for  $2D\tau^{-1}$ ;

$$2D\tau^{-1} = 1 + \frac{1}{6} \frac{l^{-1}}{\Lambda} \frac{L^{-1}}{2 + \frac{1}{3}l^{-2}}; \quad (\text{B 54})$$

where we used  $A_0 = 16F_0^0$  and  $F_0 = +i^{-1}$ . Observing this expression, notice that the second member of the r.h.s. is nothing but the quantum correction to the diffusion constant, which basically corresponds to the A WL correction to the conductivity.

#### b. form $\neq 0$ case

In the presence of relatively large topological mass, i.e.  $D l^2 \gg \frac{1}{\text{topo}}$ , the parity di usion mode becomes the high-energy degree of freedom. As such, only the first term in eq. (106) contributes the di usion. With eq. (95), such di usion is given as follows;

$$\hat{\chi}^d(q;!)_{F_5 \neq 0} = \frac{sf_4}{8} \frac{1+t^2}{2} \hat{1} + \hat{T}_4 \hat{1} + \hat{S}_1 + \frac{1}{2} \frac{t^2}{2} \hat{1} + \hat{T}_4 \hat{T}_1 + \hat{S}_2 + t \hat{T}_2 + \hat{T}_3 \hat{1} + \hat{S}_1^0; \quad (\text{B 55})$$

where  $s$  and  $t$  are defined by  $a_{04}$ ,  $a_1$  and  $a_{23}$ ;

$$a_{04} = \frac{1+t^2}{s}; \quad 3a_1 = \frac{1}{s} \frac{t^2}{2}; \quad a_{23} = st;$$

Contrary to the previous subsection, the tensor-part of the di usion depends on the model-parameters through the "tensor-form factor"  $t$ . As such, we will employ in this case not only the di usion constant  $D$  but also this tensor-form factor  $t$  as the "mean-field parameters", which should be self-consistently determined. In other words, both of them should be given by the relaxation kernels, as in eq. (B 41).

To do this, we will first calculate both the density relaxation function  $\chi_0$  and the sublattice density relaxation function  $\chi_5$ , by the use of eq. (B 55). Namely, we will substitute eq. (B 55) into eqs. (B 23, B 28), only to obtain these two functions in terms of  $sf_4$  and  $t$  first. The relaxation functions thus calculated read as follows;

$$\chi_0(q;!) = \frac{32}{32} \frac{2}{2} isf_4; \quad (\text{B 56})$$

$$\chi_5(q;!) = \frac{32}{32} \frac{2}{2} istf_4; \quad (\text{B 57})$$

Then, we will equate eqs. (B 56, B 57) with the first two members of eq. (B 40) respectively. By way of this,  $f_4$  and  $t$  can be given in terms of the relaxation kernels;

$$sf_4 = \frac{1}{32} \frac{1}{2} \frac{A_0 j}{D q^0}; \quad (\text{B 58})$$

$$t = \frac{B_0}{M_{5;5}} \frac{2iF_5^{00} + M_{5;0}}{M_{5;5}}; \quad (\text{B 59})$$

By substituting these two back into eq. (B 55), we can express the di usion only in terms of the relaxation kernels. When its hole-line time is reversed, the corresponding Cooperon is readily derived;

$$U^{\text{coop}}(k + k^0;!) = \frac{1}{2^9} \frac{1}{i^{-2}} \frac{A_0}{iD(k + k^0)^2} (1 + t^2) \hat{1} + \hat{T}_4 \hat{1} + \hat{S}_1 + (1 - t) \hat{1} + \hat{T}_4 \hat{T}_1 + \hat{S}_2 + 2t \hat{T}_2 + \hat{T}_3 \hat{1} + \hat{S}_1^0; \quad (\text{B 60})$$

The tensor-form factor  $t$  and the di usion constant  $D$  appearing in the right hand side above are already given by the relaxation kernels, via eq. (B 59) and eq. (B 41). Such relaxation kernels are given by the 2P IR vertex function (see eq. (B 30)). Thus, as in the previous subsection, we will approximate the 2P IR vertex function by eq. (B 60). In terms of this substitution, we arrive at a closed coupled equation for the di usion constant  $D$  and the tensor-form factor  $t$ , whose explicit expressions are given in the appendix C.

When solving this gap equation, we can see how the quantum correction to the di usion constant behaves as a function of  $m$  and  $\Lambda$ . Several limiting values are summarized in Fig. 18. Especially, in the zero mass limit i.e.  $m = 0+$ , the solution of the gap equation reduces to a following simple function of  $F_0 = +i^{-1}$ ;

$$\lim_{m \rightarrow 0+} 2D\tau^{-1} = 1 + \frac{1}{12} \frac{l^{-1}}{2} \frac{L^{-1}}{2 + \frac{1}{3}l^{-2}}; \quad (\text{B 61})$$

Comparing this with eq. (B 54), one can easily see that the quantum correction to the di usion constant is actually half of that for  $m = 0$  case.

The discrepancy between eq. (B 54) and eq. (B 61) is responsible for the Cooperon term associated with the parity di usion mode, i.e. the second member of the right hand side of eq. (112). To see this explicitly, note first that  $a_2$ ,  $a_3$  and  $a_4$  appearing in eqs. (113-114) reduce

FIG. 18: A summary of several limiting values of the quantum correction of the diffusion constant in the presence of the topological mass. Eq. (B 61) corresponds to the green shaded region.

to zero in the limit of  $m \rightarrow 0^+$ . Then, eqs. (113,114) in this limit read as follows;

$$\lim_{m \rightarrow 0^+} \hat{U}_1^c = \begin{array}{ccccc} & n & & & \\ & \hat{1} & \hat{T}_1 & \hat{S}_1 + \hat{S}_2 & \\ & & & & \circ \\ & + \hat{T}_4 & \hat{1} + \hat{T}_1 & \hat{S}_1 & \hat{S}_2 \end{array} ; \quad (\text{B } 62)$$

Observing these expressions, notice that the second members of both eq. (B 62) and eq. (B 63) are totally ineffective in the current-type relaxation kernels;

$$\hat{T}_4 \quad \hat{1} + \hat{T}_1 \quad \hat{S}_1 \quad \hat{S}_2 \quad \vdots \quad \hat{q}^{\wedge} = 0; \quad (B\ 64)$$

$$\hat{T}_4 \quad \hat{1} + \hat{T}_1 \quad \hat{S}_1 \quad \hat{S}_2 \quad , \quad \hat{q}^{\wedge}_5 = 0 \quad (B.65)$$

The consequence of these two equations are two-fold. The second equation in combination with eq. (B 52) leads  $M_{jj;j} = 0$  *rst.* Thus, we have  $D = \frac{i}{M_{jj}}$  again, which indicates that  $M_{jj;j}$  originated from eq. (B 62) and that from eq. (B 63) contribute to the quantum correction in an additive way. Eq. (B 64) moreover indicates that these two quantum corrections have the same magnitude and sign. In other words, the quantum correction derived in Appendix B 2a, i.e. eq. (B 54), can be divided into two parts;

$$2D_{\overline{m}=0}^1 = 1 + \frac{1}{12} \frac{L^1}{L^1} \frac{L^1}{L^1} \frac{2 + \frac{1}{2}}{2 + \frac{1}{2}} + \frac{1}{12} \frac{L^1}{L^1} \frac{L^1}{L^1} \frac{2 + \frac{1}{2}}{2 + \frac{1}{2}} :$$

Each of these two quantum corrections is originated from eq. (B 62) and eq. (B 63) respectively. Since we have already ignored eq. (B 63) for the  $m \neq 0$  case, the resulting solution has only single  $l=1,2$ , as in eq. (B 61).

APPENDIX C: MEAN-FIELD EQUATION FOR  
m  $\neq$  0 CASE

The mean-field equation for the diffusion constant  $D$  and  $t$  in the presence of the finite topological mass is given as follows;

$$D \quad \frac{i}{M_{ij} M_{5i;5j}} \frac{M_{5j;5j}}{M_{5i;ij} M_{ij;5j}}; \quad t \quad \frac{2iF_5^{00} + M_{5j;0}}{M_{5;5}};$$

with the relaxation kernels  $M_{a;b}$  being given by D and t self-consistently;

$$M_{a;b} = 2iF_0^{00} \frac{\mathcal{A}_{0j}}{2^{13} 2D} \frac{1}{2} \frac{d^3 k d^3 k^0}{j \cdot k^0 j} \frac{1}{j \cdot k^0 j} \hat{\gamma}_a^L(k) (1 + t^2) \hat{1} + \hat{T}_4 \hat{1} \hat{S}_1 (1 - t) \hat{1} \hat{T}_4 \hat{T}_1 \hat{S}_2 + 2t \hat{T}_2 + \hat{T}_3 \hat{1} \hat{S}_1, \quad \hat{\gamma}_a^R(k^0) :$$

Note that  $\wedge^{\mathbb{L};\mathbb{R}}(\mathbf{k})$  above are previously defined;

$$\begin{aligned} \hat{a}_\alpha^L(k) &= \frac{1}{2} \left( \hat{G}^L(k; 0; 0) \hat{G}^{R; -1}(k) + \hat{a}^\dagger \hat{G}^R(k) \right) \\ &+ \hat{G}^A(k) \hat{a}^\dagger \hat{G}^{A; -1}(k) - \hat{G}^L(k; 0; 0); \\ \hat{a}_\alpha^R(k) &= \hat{G}_A \hat{G}_{0; \alpha}(k); \end{aligned}$$

with  $\hat{v}_a$  for  $a = 0; 5; j$  and  $5j$  given in eq. (B 28).  $g_{00;a}(x)$  used in  $\hat{\Delta}_R^a(k)$  are given in terms of the 1-point Green

functions ( $F_0$  and  $F_5$ ) and the tensor-form factor  $t$ ;

$$\begin{aligned} g_{00;0}(\mathbf{x}) / & \frac{x^2 + (\mathcal{F}_0 \mathcal{J} + \mathcal{F}_5 \mathcal{J})}{\mathcal{J}(a + ib)^2} \frac{t(\mathcal{F}_0 \mathcal{F}_5 + \mathcal{F}_0 \mathcal{F}_5)}{x^2 \mathcal{J}}; \\ g_{00;5}(\mathbf{x}) / & \frac{tx^2}{\mathcal{J}(a + ib)^2} \frac{t(\mathcal{F}_0 \mathcal{J} + \mathcal{F}_5 \mathcal{J})}{x^2 \mathcal{J}} \frac{(\mathcal{F}_0 \mathcal{F}_5 + \mathcal{F}_0 \mathcal{F}_5)}{x^2 \mathcal{J}}; \\ g_{00;j}(\mathbf{x}) / & \frac{\mathcal{F}_0^{(0)}}{\mathcal{J}(a + ib)^2} \frac{t\mathcal{F}_5^{(0)}}{x^2 \mathcal{J}} + \frac{8}{3} \frac{ab \mathcal{F}_0^{(0)}}{\mathcal{J}(a + ib)^2} \frac{t\mathcal{F}_5^{(0)} x^2}{x^2 \mathcal{J}}; \end{aligned}$$

$$g_{00;5j}(x) / \frac{F_5^0 - tF_0^0}{j(a+ib)^2 - x^2 j} - \frac{8ab(F_5^0 - tF_0^0)x^2}{3j(a+ib)^2 - x^2 j} ;$$

with  $(a+ib)^2 = F_0^2 - F_5^2$ .

#### APPENDIX D : DERIVATION OF $g_{00;a}(x)$

Starting from the Bethe-Salpeter (BS) equation for the response function, we have derived in the section B1 the EOM's for the various types of relaxation functions. Such coupled EOM's have two features; they are closed and linearized with respect to the relaxation functions. Because of these two features, we can solve them for the relaxation functions. Out of this solution, we can relate the renormalized diusion constant with the 2P IR (two-particle irreducible) vertex function. This relation in turn becomes an essential building-block of the self-consistent loop of the diusion constant (see appendix. B).

To obtain such linearized EOM's, we need to reduce the convolution part between the 2P IR vertex function and the response function into the simple product between relaxation kernels and relaxation functions. For this purpose, we have introduced the completeness in the space of the integral variable, say  $y$  or  $w$ , associated with this convolution;

$$\int_a^X u_a(y) \mu(w) (y-w) :$$

Namely, by use of this, any convolution in principle can be decomposed into a simple product;

$$\int_a^X \int_a^Z dy f(\dots; y) g(y; \dots) = \int_a^X \int_a^Z dy f(\dots; y) \int_a^Z dw u_a(w) g(w; \dots) :$$

In the current context,  $f(\dots; y)$  corresponds to the 2P IR vertex function, while  $g(w; \dots)$  to the response function. Therefore,  $\int_a^Z dw u_a(w) g(w; \dots)$  corresponds to the relaxation kernels, while  $\int_a^Z dw u_a(w) g(w; \dots)$  does to the relaxation functions (see also Appendix. B1). The trade-off for this decomposition is therefore the sum over infinite (but countable) numbers of modes specified by  $a$ .

To be more specific, we did this decomposition systematically, based on the completeness relation of the matrices and the spherical harmonic function  $Y_{lm}(\hat{k})$ ;

$$\int_a^Z dw u_a(w) g(w; \dots) = \int_a^Z dw \int_a^X \int_a^Z dy f(\dots; y) \int_a^Z dw u_a(w) g(w; \dots) = \int_a^Z dw \int_a^X \int_a^Z dy f(\dots; y) \int_a^Z dw u_a(w) g(w; \dots) :$$

As such, the momentum integral only over the angular direction,  $\hat{k}$ , is taken, while that over its radial direction,  $|\mathbf{k}|$ , is not taken. As for the convolution with respect to this radial direction, we simply replace the  $|\mathbf{k}|$ -dependence of  $(\mathbf{k}; \mathbf{k}; \dots)$  by some real-valued function  $g(|\mathbf{k}|)$ . Namely, we rewrite the right hand side

of eq. (D1) as follows;

$$\int_a^X \int_a^Z dy f(\dots; y) \int_a^Z dw u_a(w) g(w; \dots) = \int_a^X \int_a^Z dy f(\dots; y) \int_a^Z dw u_a(w) g(w; \dots) :$$

Let us justify this treatment of the radial direction. In the response function,  $(\mathbf{k}; \mathbf{k}^0; \mathbf{q}; !)$ ,  $\mathbf{q}$  and  $!$  are associated with the external momentum and frequency for the bosonic degrees of freedom. We can take these two to be small, as far as the relaxation functions for the long wave-length and low-energy region is concerned. Then, such a response function is usually dominated by the diusion  $\hat{d}(\mathbf{q}; !)$  (see eq. (110)). As a result of this, the  $|\mathbf{k}|$ -dependence in the left hand side of eq. (D2) and its  $\mathbf{q}, !$ -dependence can be factorized at the leading order in small  $\mathbf{q}$  and  $!$ ;

$$\int_a^X \int_a^Z dy f(\dots; y) \int_a^Z dw u_a(w) g(w; \dots) = \int_a^X \int_a^Z dy f(\dots; y) \int_a^Z dw u_a(w) g(w; \dots) :$$

To see this factorization more explicitly, one can take the following steps: (i) substitute the asymptotic tensor-form of the diusion into eq. (110) and the left hand side of eq. (D3), (ii) take the integral and the sum over  $\hat{k}$ ,  $k^0$ , and in eq (D3), and (iii) retain the leading order in small  $\mathbf{q}$  and  $!$ . By way of this, one can reach the factorization given in the right hand side of eq. (D3) with a specific  $g_{lm}(|\mathbf{x}|)$ .

For example, let us follow these prescriptions in the case of zero topological mass case. Observing eq. (B43), notice first the following relation;

$$\hat{d}(\mathbf{q}; !)_{F_5=0} \hat{d}(\mathbf{q}; !)_{F_5=0} = 0 ; \quad (D4)$$

for  $= 1, 2, 3$ . Using this, one can readily checked that the diusion in this case turns out to be proportional to the unit matrix, when its right hand side is traced out;

$$\int_a^X \int_a^Z dy f(\dots; y) \int_a^Z dw u_a(w) g(w; \dots) = \frac{1}{! + iDq^2} \int_a^X \int_a^Z dy f(\dots; y) \int_a^Z dw u_a(w) g(w; \dots) :$$

As such, to obtain the normalized function  $g_{00;a}(x)$  in the massless case, we have only to calculate the following quantity up to the leading order in small  $!$  and  $\mathbf{q}$ ;

$$\int_a^X \int_a^Z dy f(\dots; y) \int_a^Z dw u_a(w) g(w; \dots) = \frac{1}{i! + Dq^2} \int_a^X \int_a^Z dy f(\dots; y) \int_a^Z dw u_a(w) g(w; \dots) :$$

For example, taking the current component as  $\hat{v}_a(q)$  above, we have;

$$\frac{\chi(k; k^0; q; !)}{k^0; ; ;} = \frac{q^n}{i! D q} \frac{1}{F_0^2 k^2} + \frac{8}{3} \frac{F_0^2 k^2}{F_0^2 k^2} + O(q^2; !):$$

Observing the right hand side, one can then convince oneself of eq. (D 3). Moreover, the normalized real-valued function  $g_{0;j}(x)$  will be obtained as in eqs. (B 50, B 51).

- <sup>1</sup> S. Murakami, N. Nagaosa and S.-C. Zhang, *Science* 301, 1348 (2003).
- <sup>2</sup> J. Sinova et al, *Phys. Rev. Lett.* 92, 126603 (2004).
- <sup>3</sup> Y. K. Kato, R. C. Myers, A. C. Gossard, and D. D. Awschalom, *Science* 306, 1910 (2004)
- <sup>4</sup> J. Wunderlich, B. Kastner, J. Sinova and T. Jungwirth, *Phys. Rev. Lett.* 94, 047204 (2005).
- <sup>5</sup> C. L. Kane and E. J. Mele, *Phys. Rev. Lett.* 95, 146802 (2005).
- <sup>6</sup> C. L. Kane and E. J. Mele, *Phys. Rev. Lett.* 95, 226801 (2005).
- <sup>7</sup> B. A. Bernevig and S.-C. Zhang, *Phys. Rev. Lett.* 96, 106802 (2006).
- <sup>8</sup> Y. Hatsugai, *Phys. Rev. Lett.* 71, 3697 (1993).
- <sup>9</sup> C. Wu, B. A. Bernevig and S.-C. Zhang, *Phys. Rev. Lett.* 96, 106401 (2006).
- <sup>10</sup> C. Xu and J. E. Moore, *Phys. Rev. B* 73, 045322 (2006).
- <sup>11</sup> L. Fu and C. L. Kane, *Phys. Rev. B* 74, 195312 (2006).
- <sup>12</sup> T. Fukui and Y. Hatsugai, *Phys. Rev. B* 75, 121403(R) (2007).
- <sup>13</sup> B. A. Bernevig, T. L. Hughes and S.-C. Zhang, *Science* 314, 1757 (2006).
- <sup>14</sup> M. Konig, S. Wiedmann, C. Brune, A. Roth, H. Buhmann, L. W. Molenkamp, X. L. Qi and S.-C. Zhang, *Science* 318, 766 (2007).
- <sup>15</sup> L. Fu, C. L. Kane and E. J. Mele, *Phys. Rev. Lett.* 98, 106803 (2007).
- <sup>16</sup> R. Roy, cond-mat/0607531.
- <sup>17</sup> J. E. Moore and L. Balents, *Phys. Rev. B* 75, 121306 (R) (2007).
- <sup>18</sup> S. Murakami, *Phys. Rev. Lett.* 97, 236805 (2006).
- <sup>19</sup> D. Hsieh et al, *Nature* 452, 970, (2008).
- <sup>20</sup> Jeffrey C. Y. Teo, Liang Fu, and C. L. Kane, *Phys. Rev. B* 78, 045426 (2008).
- <sup>21</sup> A. P. Schnyder, S. Ryu, A. Furusaki, and A. W. W. Ludwig, arXiv:0803.2786
- <sup>22</sup> E. Abrahams, P. W. Anderson, D. C. Licciardello and T. V. Ramakrishnan, *Phys. Rev. Lett.* 42, 673 (1979)
- <sup>23</sup> D. Vollhardt and P. Wölfle, *Phys. Rev. Lett.* 45 842 (1980); *Phys. Rev. B* 22, 4666 (1980).
- <sup>24</sup> S. Murakami, *New J. Phys.* 9, 356 (2007); (Corrigendum) *ibid.* 10, 029802 (2008)
- <sup>25</sup> S. Murakami and S. Kuga, arXiv:0806.3309 (2008).
- <sup>26</sup> M. Onoda, Y. Avishai and N. Nagaosa, *Phys. Rev. Lett.* 98, 076802 (2007).
- <sup>27</sup> H. Obuse, A. Furusaki, S. Ryu and C. Mudry, *Phys. Rev. B* 76, 075301 (2007).
- <sup>28</sup> A. M. Essin and J. E. Moore, *Phys. Rev. B* 76 165307 (2007).
- <sup>29</sup> P. M. Ostrovsky, I. V. Gomyi, and A. D. Mirlin, *Phys. Rev. Lett.* 98, 256801 (2007).
- <sup>30</sup> S. Ryu, C. Mudry, H. Obuse, and A. Furusaki, *Phys. Rev. Lett.* 99, 116601 (2007)
- <sup>31</sup> K. Nomura, M. Koshino, S. Ryu, *Phys. Rev. Lett.* 99, 146806 (2007).
- <sup>32</sup> J. H. Bardarson, J. Tworzydło, P. W. Brouwer and C. Wu, J. Beenakker, *Phys. Rev. Lett.* 99, 106801 (2007).
- <sup>33</sup> H. Aoki and T. Ando, *Phys. Rev. Lett.* 54, 831 (1985).
- <sup>34</sup> Although the previous numerical studies done by Onoda et al.<sup>26</sup> are about the 2-dimensional case, we expect that this phase diagram holds true both in the 2-d  $Z_2$  QSH systems and in the 3-d  $Z_2$  QSH systems.
- <sup>35</sup> R. Shindou et al, in progress.